sustainability

MDPI

Article

Stability of Deep Underground Openings through Large Fault Zones in Argillaceous Rock

Deyu Qian [1,*], Nong Zhang [1,*], Dongjiang Pan [1], Zhengzheng Xie [1], Hideki Shimada [2], Yang Wang [1,3], Chenghao Zhang [1] and Nianchao Zhang [4]

1 Key Laboratory of Deep Coal Resource Mining, Ministry of Education of China, School of Mines, China University of Mining and Technology, Xuzhou 221116, China; cumtpdj@163.com (D.P.); xiezhengzheng0327@163.com (Z.X.); wangyangknowledge@126.com (Y.W.); zhangchenghao421@126.com (C.Z.)

2 Department of Earth Resources Engineering, Faculty of Engineering, Kyushu University, Fukuoka 819-0395, Japan; shimada@mine.kyushu-u.ac.jp

3 School of Public Policy and Urban Affairs, College of Social Sciences and Humanities, Northeastern University, Boston, MA 02115, USA

4 School of Earth Sciences, University of Queensland, St Lucia, QLD 4072, Australia; znc357711543@hotmail.com

* Correspondence: qiandeyu6217@163.com (D.Q.); zhangnong@126.com (N.Z.)

Received: 11 November 2017; Accepted: 21 November 2017; Published: 22 November 2017

Abstract: The stability of underground openings is pivotal to sustainable safe mining in underground coal mines. To determine the stability and tunneling safety issues in 800-m-deep underground openings through large fault zones in argillaceous rocks in the Guqiao Coal Mine in East China, the pilot industrial test, laboratory experimentation, and field measurements were used to analyze the large deformations and failure characteristics of the surrounding rock, the influence factors of safe excavation and stability of underground openings, and to study the stability control countermeasures. The main factors influencing the stability and tunneling safety include large fault zones, high in situ stress, poor mechanical properties and engineering performance of the argillaceous rock mass, groundwater inrush and gas outburst. According to the field study, the anchor-ability of cables and the groutability of cement-matrix materials in the argillaceous rock in the large fault zones were extremely poor, and deformations and failure of the surrounding rock were characterized by dramatic initial deformation, high long-term creep rate, obviously asymmetric deformations and failure, rebound of roof displacements, overall loosened deformations of deep surrounding rock on a large scale, and high sensitivity to engineering disturbance and water immersion. Various geo-hazards occurred during the pilot excavation, including roof collapse, groundwater inrush, and debris flow. Control techniques are proposed and should be adopted to ensure tunneling safety and to control the stability of deep underground openings through large fault zones, including regional strata reinforcement technique such as ground surface pre-grouting, primary enhanced control measures, floor grouting reinforcement technique, and secondary enclosed support measures for long-term stability, which are critical for ensuring the sustainable development of the coal mine.

Keywords: deep underground opening; argillaceous rock; fault zones; coal mine; excavation; deformation; grouting; stability

1. Introduction

Sustainable mining of coal resources will inevitably shift from shallow to deep within the earth's crust in China. The shallow resources are limited and are being exhausted, as the demand for and dependence on energy resources stemming from China's quick economic development and industrialization have caused the growth of coal production and consumption [1–4]. Coal accounted

for 75.6% and 66.0% of China's total energy production and consumption in 2013, respectively [5]. Coal has and will continue to occupy the dominant position in China's long-term energy mix given the rich coal resources and poor oil and natural gas resources [6–8].

With the increasing demand for energy and mining intensity, the mining depth of underground coal mines in China has increased 8–12 m per year on average. Particularly, the mining depth in East China increases by 10–25 m/year on average [2]. Approximately 200 underground coal mines presently exist, the mining depths of which have exceeded 800 m in the mining areas of Huainan, Kailuan, Xinwen, Shenyang, Changguang, Jixi, Fushun, Fuxin, and Xuzhou. Moreover, 47 underground coal mines exist in China with mining depths of more than 1000 m. The kilometer-deep coal mines in China are mainly found in the North, East, and Northeast, 80.85% of which are in East China, including the Anhui, Jiangsu, and Shandong Provinces. Among these is the Guqiao Coal Mine, which has a maximum annual coal output of 12.3 million tons (Mt) in the Huainan mining area, and the Suncun Coal Mine, which has the greatest mining depth of 1501 m in the Xinwen mining area. These are the largest kilometer-deep coal mine and the deepest coal mine in Asia, respectively. Deep underground coal resource development is being demanded by the national energy strategy.

The deep coal mines in the mining areas of East China have complex geological conditions, with thick Cenozoic loose strata, large overburden depth of coal seams, and Ordovician-confined aquifers at the bottom. The coal-series strata belong to a Carboniferous-Permian system sedimentary environment of the North China platform type. Over time, the coal seam situation and geological conditions of the coal-series strata have been affected by the Indosinian movement, Yanshan movement, Himalayan tectonic movement, and neo-tectonic movements. Faults and folds are well developed. For example, the Huainan mining area is a coalfield with the most complex geological conditions. Eighty-three large faults with throws greater than 50 m high, more than 4900 faults with throws greater than 5 m high, and many other small faults in the Huainan mining area have been found [9].

Faults are commonly encountered poor geological conditions during underground excavation [10]. Deformations and failure of an underground opening are prominently governed by adjacent faults [10,11]. In engineering practices, many instability problems, including underground openings during excavation and operation, are caused by these deformations and failures regardless of fault exposure or concealment during excavation [12,13]. Some experts and scholars have analyzed the surrounding rock stability of underground openings or tunnels affected by faults. Numerical and physical simulation analyses have revealed that the extent of deformation and the size of the plastic zone increased as the distance from a fault to the tunnel decreased, and the shear deformation occurred along the weak plane [14]. Numerical investigation using Universal Distinct Element Code (UDEC) software indicated that a fault affects the stability of an underground opening by increasing the plastic zones and displacements, and by causing asymmetrically distribution in rock masses adjacent to the excavation [12]. Using an articulated design for the lining was proposed for a motorway tunnel through an active fault zone in Turkey to mitigate the seismic risk [15]. The freezing construction method was used in the Guangzhou metro tunnel crossing the Qingquanjie fault [16]. Based on monitoring analysis of the main haulage roadway at a mining level of −648 m through a large fault, floor heave was an important factor for instability and failure of the roadway. The grouting tube and rock bolts at wall corners were used to resist the shear displacement at the floor corner with concentrated stress [10]. Support schemes of the surrounding rock, including 2–3 m-long advance pre-grouting, shotcrete, shedding, and bolts, were proposed to control the stability of a main roadway through a large aquitard normal fault F92 with 435 m-high throw in the Taoyuan Coal Mine in China [17].

Previous control techniques of the surrounding rock in underground engineering have mainly focused on a single fault fracture zone or fault zones at shallow depths. However, few studies have been performed on the stability control of deep underground openings through large fracture zones of fault groups (fault zones) in areas with high in situ stress. Currently, no completely successful engineering examples have reported safety and long-term stability of underground openings 800 m or deeper below the ground surface through large thick fault zones. When underground openings,

such as tunnels, are excavated through large thick fault zones, construction accidents, such as the collapse of large rock mass volume into the opening, may suddenly and unexpectedly occur because of the extremely variable lithology, complexity, and mutability of geological conditions. This causes considerable difficulties for the construction and property losses but also seriously threatens the lives of workers. Using conventional surrounding rock control techniques, avoiding geo-hazards such as roof collapse, groundwater inrush, debris flow, etc., during excavation is difficult. Progressive instability and failure of the surrounding rock and support structure during operation may be a result of long-term creep and time-dependent behavior, especially in deep underground openings through large thick fault zones in argillaceous rock. The tunneling safety and stability of underground openings or gateroads are vital for ventilation, transportation and other essential services for sustainable safe mining of underground coal mines [18,19].

Based on the engineering background of underground openings at a depth of 800 m below the ground surface, through large fault zones in argillaceous rock in the Guqiao Coal Mine in the Huainan mining area, the pilot industrial test, laboratory experiment, and field measurements methods were used to analyze the deformation and failure characteristics of the surrounding rock, reveal the factors that influence safe excavation and underground opening stability, and study the proposed control countermeasures for safe excavation and stability. The originality of this study includes the minimum range of pre-grouting and post-grouting reinforcement for deep underground openings through large fault zones, pre-grouting and deep holes post-grouting with a novel polyurethane grouting material, and floor grouting reinforcement technique. The main objectives are to propose safe excavation and stability control techniques for deep underground opening through large fault zone in argillaceous rock. This study has practical referable significance for deep underground openings through large fault zones, especially in underground coal mines in East China, as well as other deep underground engineering scenarios with similarly complex geological conditions.

2. Geological Profiles of Deep Underground Openings in Large Fault Zones

2.1. Introduction to the Guqiao Coal Mine

The Guqiao Coal Mine is in the Northwest of Huainan City, Anhui Province, 500 km from Shanghai City, China. It is one of the major coal mines owned by Huainan Mining (Group) Co., Ltd., Huainan, China, that provides an important energy source for the rapid sustainable economic growth of East China [20], producing an annual coal output of more than 11 million tons (Mt) since 2009, reaching a maximum of 12.3 Mt/year. The mine is expected to have a remaining service life of up to 85 years as of 2013. The coal mine is divided into four districts: central, eastern, northern, and southern. The recoverable reserves within the southern district are 392.7 million tons, accounting for 30.3% of the total recoverable reserves of 1297 million tons in the Guqiao Coal Mine.

2.2. Geological Profiles of Deep Underground Openings

The south haulage and rail underground openings, with a horizontal width of 30–40 m in the first mining level of −780 m, connect the central mining district to the southern mining district as two key transportation corridors playing a pivotal role in the sustainable development of the Guqiao Coal Mine with high output. The south underground openings, with a length of 3000 m, inevitably pass through large geological anomaly fault zones within the southern "X" conjugate shear fault zones where many numerous fault structures exist that are extremely complex, as shown in Figure 1.

According to drill core logs and surface geological boreholes (SGB), the rock quality designation (RQD) values (Figure 2) are generally less than 25%, and the RQD is zero within the fault fracture zones, reflecting that the fault zones and adjacent rock mass are extremely broken. The pilot underground excavation passing through fault FD108-1 also showed that small faults and fractures are well-developed, and the surrounding rock is generally broken. The lithology is mainly made of argillaceous rock mass. The rock mass contains dense fractures, most of which are filled with fault gouge and argillaceous infilling.

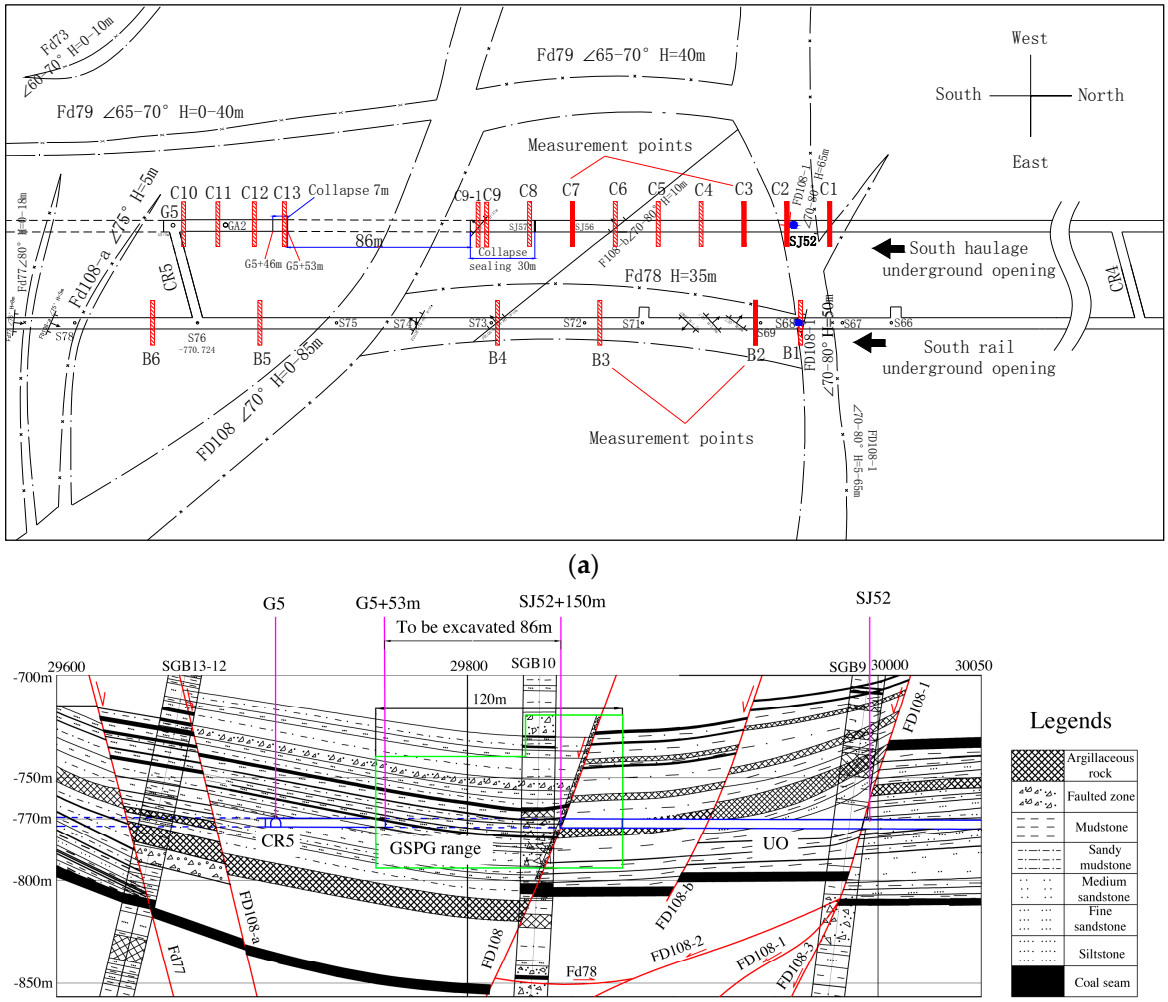

(**a**)

*(1) UO: Underground opening; (2) GSPG: Ground surface pre-grouting, Length:120m,Width:37, Roof: 30m or 50m, Floor: 20m; (3)SGB: surface geological borehole; (4) CR5: Connection roadway; (5) FD108-1 ∠70° H=65m, FD108-b ∠70° H=10m, FD108 ∠70-80° H=37m, FD108-a ∠75° H=5m, Fd77 ∠75° H=8m, FD108-2 ∠45-50° H=5-35m, FD108-3 H=35m, F78 H=35m

(**b**)

Figure 1. (**a**) Plan of the geological profiles of the underground openings and field measurement points during the pilot excavation of the Guqiao Coal Mine. Note: CR5: Connection roadway No. 5; CR4: Connection roadway No. 4; SJ52 and S68 are two geological observation points at the interface between the geological anomaly fault zones and normal locations in the south haulage and the rail underground openings, respectively. (**b**) Section of geological profiles of the haulage underground opening in the Guqiao Coal Mine. Note: Ground surface pre-grouting (GSPG) reinforcement range outlined in the green box was completed after the pilot excavation and before re-excavation.

The underground excavation will involve the geological anomaly fault zones consisting of a series of faults from the north to the south, including FD108-1 (normal faults, dip angle: 70°–80°, throw height H = 65 m, the width of aperture with fillings of clay fault gouge W = 4.3 m), FD108-b (normal fault, dip angle: 70°–80°, H = 10 m), FD108 (normal fault, dip angle: 70°–80°, H = 37 m, W = 12 m), FD108-a (normal fault, dip angle: 75°, H = 5 m), Fd77 (normal fault, dip angle: 75°, H = 0–18 m), etc. The structural form in the section is a large graben made up of the eight main step-shaped normal faults with an east–west (EW) direction on the strike and a dip in the south–north (SN) direction. The maximum combined drop of 140 m of the fault group is 670 m wide from north to south. The structures are well-developed in the fault zones. Moreover, the groundwater pressures within the large fault zones are high [21].

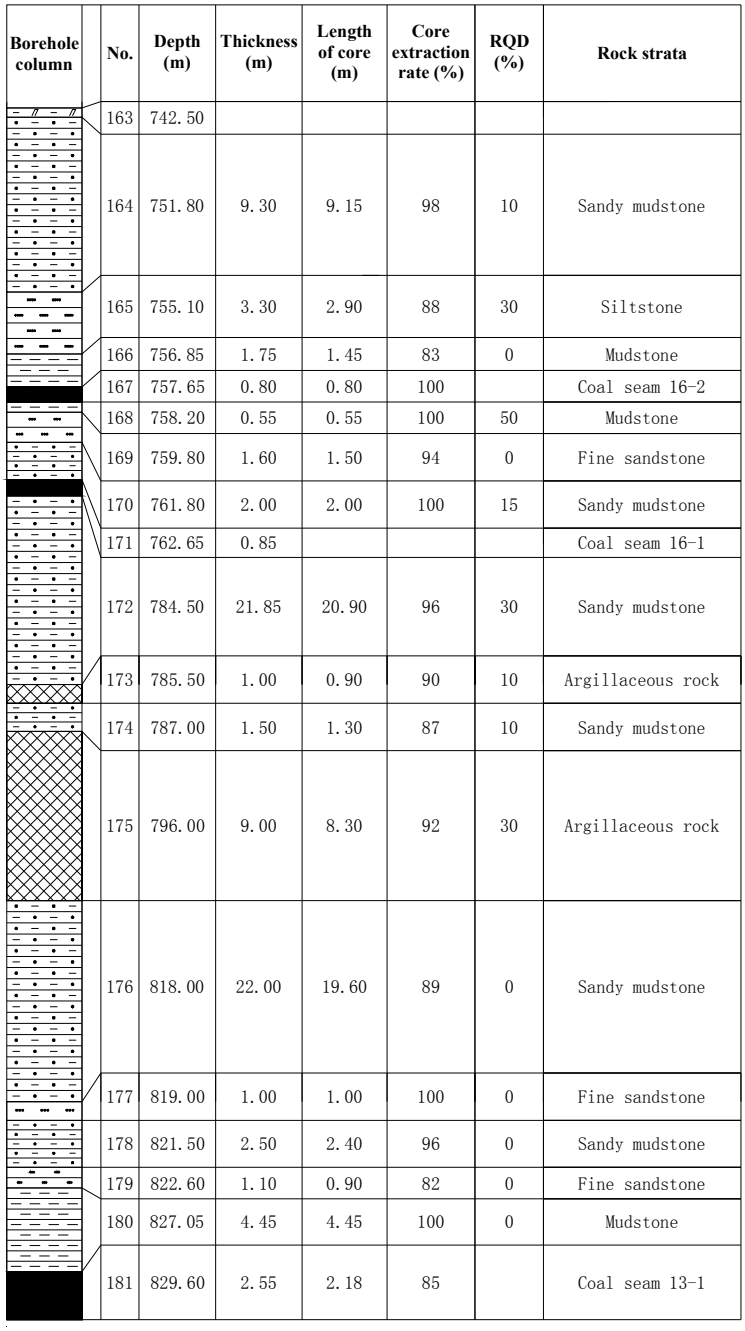

Borehole column	No.	Depth (m)	Thickness (m)	Length of core (m)	Core extraction rate (%)	RQD (%)	Rock strata
	163	742.50					
	164	751.80	9.30	9.15	98	10	Sandy mudstone
	165	755.10	3.30	2.90	88	30	Siltstone
	166	756.85	1.75	1.45	83	0	Mudstone
	167	757.65	0.80	0.80	100		Coal seam 16-2
	168	758.20	0.55	0.55	100	50	Mudstone
	169	759.80	1.60	1.50	94	0	Fine sandstone
	170	761.80	2.00	2.00	100	15	Sandy mudstone
	171	762.65	0.85				Coal seam 16-1
	172	784.50	21.85	20.90	96	30	Sandy mudstone
	173	785.50	1.00	0.90	90	10	Argillaceous rock
	174	787.00	1.50	1.30	87	10	Sandy mudstone
	175	796.00	9.00	8.30	92	30	Argillaceous rock
	176	818.00	22.00	19.60	89	0	Sandy mudstone
	177	819.00	1.00	1.00	100	0	Fine sandstone
	178	821.50	2.50	2.40	96	0	Sandy mudstone
	179	822.60	1.10	0.90	82	0	Fine sandstone
	180	827.05	4.45	4.45	100	0	Mudstone
	181	829.60	2.55	2.18	85		Coal seam 13-1

Figure 2. Rock quality designation (RQD) Values and borehole core column of surface geological borehole No. 10 (SGB10).

3. Deformations, Failure Characteristics, and Factors Influencing Deep Underground Openings through Large Fault Zones

3.1. Profiles of Industrial Test of the Pilot Excavation of Deep Underground Openings

The south underground opening with a quadrant angle of NS178° (azimuth of 358°) was excavated along an uphill slope of 3‰ at a depth of approximately 800 m below the ground surface. Its cross-section has a semicircle-arch crown shape with a straight sidewall. The excavation cross-section was 6000 mm wide and 4600 mm high, whereas the cross-section after the use of U-shaped steel sets and shotcrete support was 5600 mm wide and 4400 mm high. Many support schemes

were used and optimized during the industrial testing of the pilot excavation of the underground openings through the large geological anomaly fault zones, such as the single pilot heading method (small cross-section: 4600 mm wide and 3500 mm high) and 35 m-long boreholes pre-grouting. However, various geo-hazards still occurred during the previous excavation, including roof collapse, groundwater inrush, and debris flow, which seriously threatened tunneling safety in the deep underground openings. Several main optimization support schemes during the pilot excavation were used as follows.

(1) Scheme 1 (SJ52~SJ52 + 80 m, G5~G5 + 46 m in the south haulage underground opening; S68~Fault F108 in the south rail underground opening): Five 3 m-long advanced boreholes pre-grouting with rapid-hardening high-strength sulfoaluminate cement (with a strength grade of 52.5 MPa) and U29-shaped steel sets support with intervals of 500 mm, plus 19 high-strength bolts reinforcing each cross-section (array pitch was 1000 mm), primary shotcrete with a thickness of 70 to 100 mm and seven pre-stressed cables (length of 6300 mm and a diameter of 17.8 mm) supporting the roof and sidewalls (the array pitch was 1000 mm), and secondary shotcrete with a thickness of 50 mm, plus post-grouting (1.5 m-deep holes, 3 m-deep holes, and supplementary 8 m-deep holes post-grouting with ordinary Portland cement with a strength grade of 42.5 MPa).

(2) Scheme 2 (SJ52 + 80 m~SJ52 + 150.8 m, G5~G5 + 46 m in the south haulage underground opening): Five 8 m-long advanced boreholes pre-grouting with sulfoaluminate cement, U29-shaped steel sets support with intervals of 500 mm, primary shotcrete with a thickness of 70–100 mm, 17 bolts and seven cables reinforcing each cross-section, secondary shotcrete with a thickness of 50 mm, and post-grouting (3 m-deep holes with ordinary Portland cement and 8 m-deep holes with superfine cement with a strength grade of 62.5 MPa). The specifications of the bolts were the same as those of Scheme 1. The interval and array pitch of the bolts were 800 mm and 1000 mm, respectively. The diameter and length of the cables were 21.8 mm and 6300 mm, respectively. The array pitch of the cables was 1000 mm.

(3) Scheme 3 (SJ52 + 120 m~SJ52 + 150 m in the south haulage underground opening): 35 m-long borehole grouting (the grouting material was ordinary Portland cement with a strength grade of 52.5 MPa and sodium silicate), U36-shaped steel sets support with intervals of 500 mm, plus bolts and cables, shotcrete with a thickness of 70–100 mm, and post-grouting (3 m-deep hole with ordinary Portland cement and 8 m-deep hole with superfine cement). The parameters of the bolts, cables, and post-grouting were the same as those in Scheme 2.

(4) Scheme 4 (Fault FD108 at SJ52 + 148.8 m~SJ52 + 154 m in the south haulage underground opening): Five advanced exploration boreholes (25–75 m long) and six gas and water drainage boreholes (46–49 m long), 30 m-long boreholes pre-grouting (the grouting material was ordinary Portland cement with a strength grade of 52.5 MPa and sodium silicate (3–5% by weight)), 15 m-long shed-pipe advanced pre-grouting support, 8 m-long boreholes pre-grouting with Gurit chemical material, U36-shaped steel sets support with intervals of 500 mm, shotcrete with a thickness of 70–100 mm and 3 m-deep holes post-grouting with ordinary Portland cement, plus cables, and 8 m-deep holes post-grouting with superfine cement. The parameters of the cables and post-grouting were the same as those in Scheme 2.

(5) Scheme 5 (G5 + 46 m~G5 + 53 m in the south haulage underground opening and from Fault F108 at S68, and 200 m to the south in the south rail underground opening): 8 m-long boreholes pre-grouting with sulfoaluminate cement, single-pilot heading method with a small cross-section 4600 mm wide and 3500 mm high, U36-shaped steel sets with intervals of 500 mm, shotcrete with a thickness of 70–100 mm, 3 m-deep holes with high strength sulfoaluminate cement, 13 bolts and five cables supporting each cross-section (the bolts and cables had a diameter of 22 mm and a length of 2800 mm, and a diameter of 21.8 mm and a length of 7300 mm, respectively. The array pitches of the bolt and cable layouts were both 1000 mm), and 8 m-deep holes post-grouting with superfine cement.

The roof collapse and debris flow occurred in the areas from SJ52 + 120 m to SJ52 + 150 m in the south haulage underground opening when the tunneling face approached fault FD108 under the support of Scheme 2. The instantaneous volume of debris flow was up to 20 m^3. The areas were then sealed, and 88.75 t sulfoaluminate cement was used to infill the roof collapse space. After that, Scheme 3 was used, but the roof collapse and debris flow occurred once more when the tunneling face approached fault FD108. Afterward, Scheme 4 was used. However, the northern roof collapse and debris flow occurred again.

The roof collapse occurred in the south rail underground opening under support Scheme 1 when the tunneling face reached fault FD108. Scheme 5, including the 8 m-long borehole pre-grouting and pilot heading method, was then used in the south rail underground opening from fault FD108 toward the south. Nevertheless, the southern roof collapse occurred again when Scheme 5 was used as the tunneling face approached the G5 + 53 m area in the south haulage underground opening. The roof collapse in the south underground opening is shown in Figures 3 and 4.

Figure 3. The debris flow and roof collapse at the tunneling face near fault FD108.

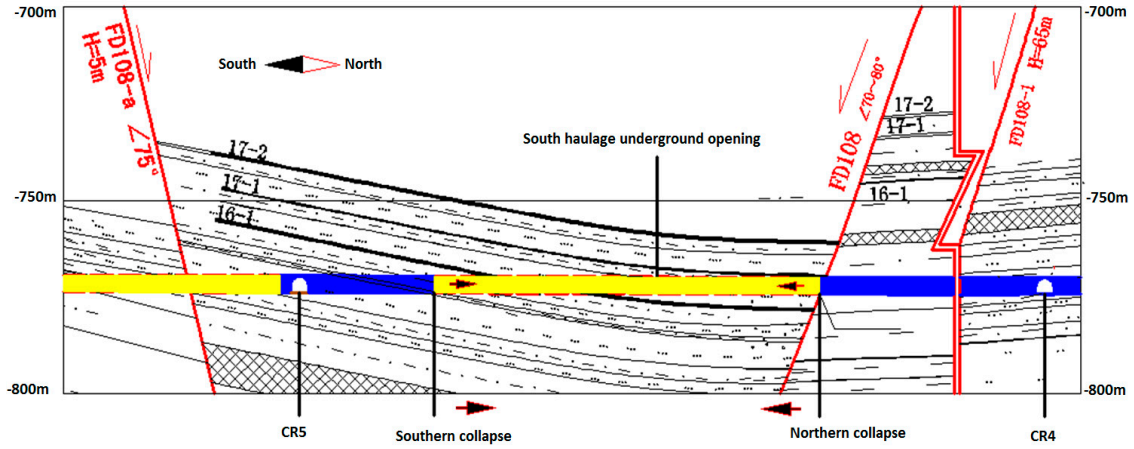

Figure 4. The collapse section diagram of the south haulage underground opening.

In addition, other geo-hazards were encountered, and special phenomena occurred during excavation. Orifice flow and groundwater inflow occurred while drilling the advanced exploration, gas, and groundwater drainage boreholes. The distance of the orifice flow including coal, water, and gravel from the borehole was more than 10 m. The maximum orifice flow from a single advanced exploration borehole was up to 14 m^3. The maximum gas concentration in the advanced geological boreholes was up to 10%. The sticking, blocking, and jamming of drill bits frequently occurred during the advanced exploration drilling process and pre-grouting boreholes.

3.2. Deformations and Failure Characteristics of Deep Underground Openings

The pressure and deformation behaviors of the underground openings were changeable because of the extremely complex and variable lithology in the large fault zones. Field measurements, such as surface displacements using the M9579-YHJ-300J (A) laser distance measurement instrument with the accuracy of 1 mm, axial load of bolts and cables, and borehole image monitoring, were performed during the pilot excavation to analyze the pressure on the support structure and deformation behavior law of the surrounding rock and evaluate the effect and rationality of various support measures. The layout of the field measurement points during the pilot excavation is shown in Figure 1. The displacements of the surrounding rock at the representative measurement points C3 at SJ52 + 24 m and C7 at SJ52 + 104 m are graphically presented in Figures 5 and 6.

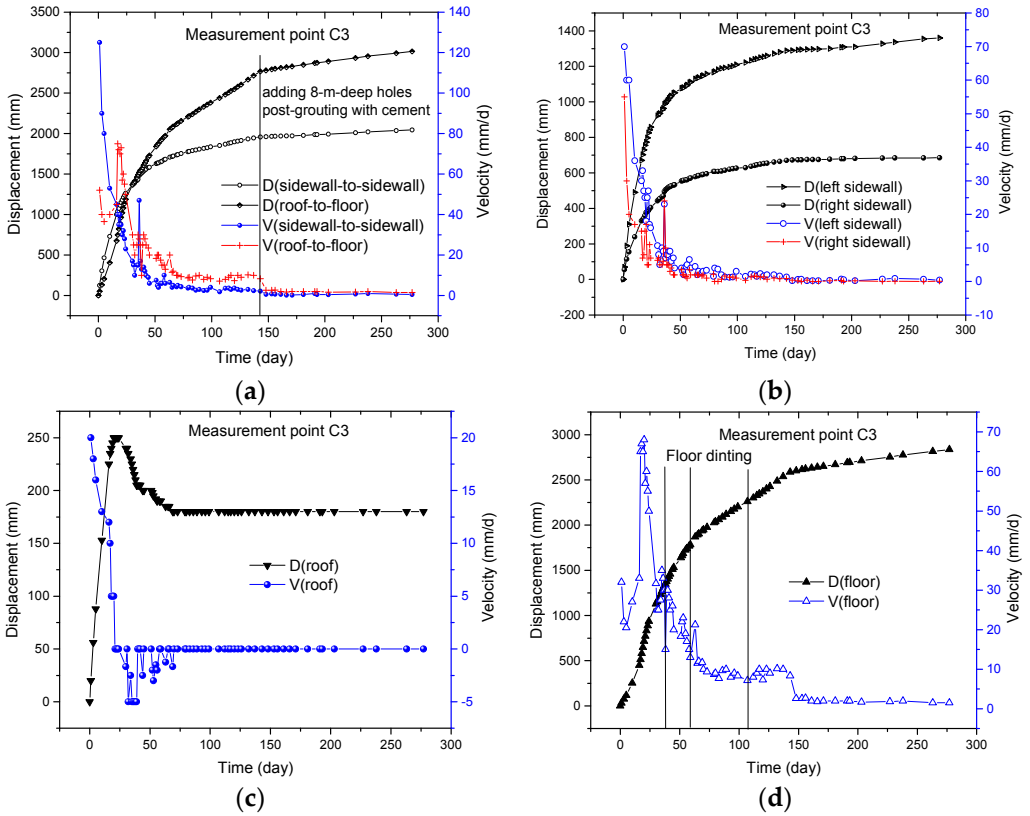

Figure 5. Curves of displacements and velocities versus time at measurement point C3: (**a**) sidewall-to-sidewall and roof-to-floor; (**b**) left and right sidewalls; (**c**) roof; and (**d**) floor.

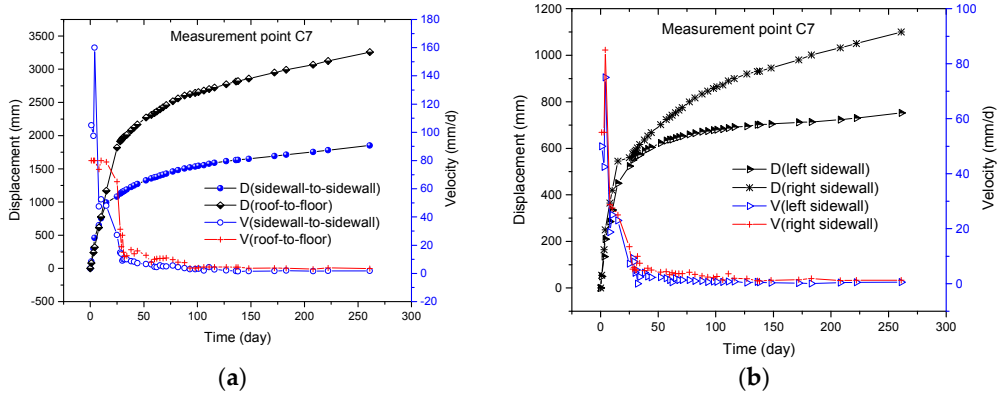

Figure 6. *Cont.*

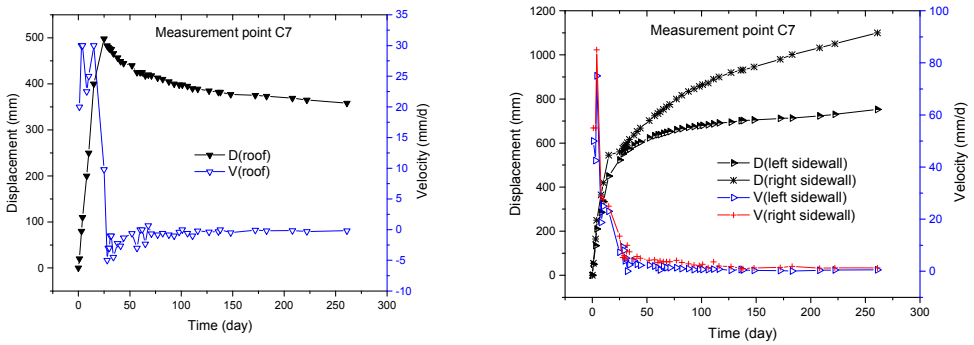

Figure 6. Curves of displacements and velocities versus time at measurement point C7: (**a**) sidewall-to-sidewall and roof-to-floor; (**b**) left and right sidewalls; (**c**) roof; and (**d**) floor.

3.2.1. Dramatic Initial Deformations

The sidewall-to-sidewall and roof-to-floor displacements were severe at the early stage due to a redistribution of stresses in the rock mass around the opening resulting from the excavation [22]. The visible macroscopic deformations and support structure damage occurred half a month after excavation. For example, according to the monitoring results of measurement point C3, the maximum displacement velocities of sidewall-to-sidewall and roof-to-floor were 125 mm/day and 75 mm/day, respectively (Figure 5a). Sixteen days later, the sidewall-to-sidewall and roof-to-floor displacements were 1000 mm and 675 mm, respectively, and the corresponding displacement velocities were 58.33 mm/day and 41.53 mm/day, respectively.

Similarly, according to the monitoring results of measurement point C7, the maximum velocities of sidewall-to-sidewall and roof-to-floor displacement were 160 mm/day and 80 mm/day, respectively (Figure 6a). Fifteen days later, the sidewall-to-sidewall and roof-to-floor displacements were 995 mm and 1170 mm, respectively, and the corresponding displacement velocities were up to 48 mm/day and 79 mm/day, respectively.

The duration of the dramatic initial deformation stage was approximately 70 days. Seventy days later, the sidewall-to-sidewall and roof-to-floor displacements and velocities at measurement point C3 were 1740 mm and 2128 mm, 5 mm/day and 10 mm/day, respectively (Figure 5a). Likewise, the corresponding displacements and velocities at measurement point C7 were 1427 mm and 2460 mm, 5 mm/day and 11 mm/day, respectively (Figure 6a).

3.2.2. High Long-Term Creep Rate

The surrounding rock tended to deform gently and smoothly after the stress redistribution disturbance and relatively rapid initial deformation. According to the monitoring at measurement point C3 and construction information on site, the supplementary 8 m-deep holes post-grouting with cement in Scheme 1 was further completed on the 143rd day, when the sidewall-to-sidewall and floor creep rates were 2.17 mm/day and 8.33 mm/day, respectively, which then dropped to 0.6 mm/day and 2.60 mm/day, respectively, on the 148th day (Figure 5a,d). The 8 m-deep holes post-grouting reinforced the surrounding rock and improved the anchor effect of the cables to some extent, which decreased the deformation creep rates.

However, a significant time-dependent creep behavior of argillaceous surrounding rock still occurred, which would lead to the progressive damage and delayed failure that undermine the long-term stability of underground openings [23]. The effect of the 8 m-deep holes post-grouting with cement was limited. Specifically, a total of 277 days later, the creep rates of sidewall-to-sidewall, roof-to-floor, the left sidewall, the right sidewall, the roof, and the floor at measurement point C3 were 0.50 mm/day, 1.50 mm/day, 0.43 mm/day, 0.07 mm/day, 0 mm/day, and 1.50 mm/day, respectively. The total corresponding displacements were 2045 mm, 3015 mm, 1360 mm, 685 mm, 180 mm, and 2835 mm, respectively (Figure 5).

With respect to measurement point C7, the total displacements of 1852 mm, 3259 mm, 752 mm, 1100 mm, 358 mm, and 2901 mm were recorded for sidewall-to-sidewall, roof-to-floor, the left sidewall, the right sidewall, the roof, and the floor, respectively, for a monitoring period of 261 days after excavation. The corresponding creep rates were 1.85 mm/day, 3.49 mm/day, 0.56 mm/day, 1.28 mm/day, −0.18 mm/day, and 3.67 mm/day, respectively (Figure 6). The creep deformation of the deep underground openings in argillaceous rock could be perpetual and last as long as the opening exists or even after full closure occurs. The high long-term creep rate indicates that support schemes 1 and 2 do not meet the requirements for long-term stability of the underground openings. The obvious creep and time-dependent behavior of deep underground openings in argillaceous rock are due to the solid–liquid–gas-temperature coupling effect of deep rock mass and the interaction with the underground openings, which is a complex issue that should be further investigated.

3.2.3. Obviously Asymmetric Deformations

The northern 150 m-long pilot excavation of the south haulage underground opening was between the large faults FD108-1 and FD108. Moreover, two strike faults, Fd78 and Fd79, were approximately parallel to the opening axis direction that were on the east and west sides of the opening, respectively.

The deformations and failure of the surrounding rock showed significant asymmetry on the same cross-section along the axis direction due to the influence of the fault group. More precisely, the deformation of the left sidewall (1360 mm) was greater than that of the right sidewall (685 mm), which accounted for 67% of the sidewall-to-sidewall closure (2045 mm) in the area from SJ52 to SJ52 + 80 m (Figure 5a,b). Conversely, the deformation of the right sidewall (1100 mm) was greater than that of the left sidewall (752 mm), representing 59% of the sidewall-to-sidewall closure (1852 mm) in the area from SJ52 + 80 m to SJ52 + 150 m (Figure 6a,b). The floor deformations at measurement points C3 and C7 accounted for 94% and 89% of the corresponding roof-to-floor convergences, respectively, which were much greater than that of sidewall-to-sidewall, which was much larger than that of the roof. The asymmetric failure of the surrounding rock and support structure are shown in Figure 7.

Figure 7. The asymmetric failure of the surrounding rock and support structure: (**a**) left sidewall from SJ52 to SJ52 + 80 m; (**b**) right sidewall from SJ52 + 80 m to SJ52 + 150 m; and (**c**) severe floor heave.

3.2.4. Rebound Phenomenon of Roof Displacements

The rebound phenomenon of roof displacements occurred 30 days after the pilot excavation (Figures 5c and 6c). For instance, the roof displacement velocity at measurement point C3 experienced a fluctuation between −5.0 mm/day and 0 mm/day from 30 days to 70 days after excavation (Figure 5c). Afterward, the roof displacement tended to be stable. This is perhaps because many developing fissures and pore spaces exist in the roof rock mass. The roof experienced an upward movement trend under the squeezing action of high horizontal tectonic stress and the large sidewall-to-sidewall deformations.

3.2.5. High Sensitivity to Engineering Disturbance and Water Immersion

According to the construction information and continuous monitoring, the displacement velocities increased due to the floor dinting, the adjacent excavation, groundwater or construction water

immersion, and blasting operation. The curve of the displacement velocities showed an obvious fluctuation during excavation due to engineering disturbance and water immersion (Figures 5 and 6). For example, the floor dinting around measurement point C3 occurred on the 38th day and 59th day, when the displacement velocities of the floor were 15 mm/day and 13 mm/day, respectively. In contrast, the displacement velocities suddenly accelerated to 30 mm/day on the 39th day and 21 mm/day on the 63rd day (Figure 5d).

3.2.6. Overall Loosened Deformations of Deep Surrounding Rock on a Large Scale

Multiple-point borehole extensometers were installed in both sidewalls (Figure 8) at measurement point B2 in the south rail underground opening to obtain the displacements of the deep surrounding rock mass.

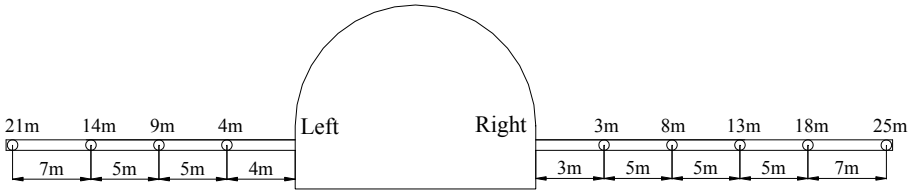

Figure 8. Layout of multiple-point borehole extensometers at measurement point B2.

The absolute displacements of the 4 m-deep point, 9 m-deep point, and 14 m-deep point within the left sidewall were 93, 52, and 14 mm, respectively, which accounted for 61%, 34%, and 9% of the total displacement of 153 mm between 0 m and the 21-m-deep point, respectively (Figure 9a). The absolute displacements of the 3 m-deep, 8 m-deep, 13 m-deep, and 18-m-deep points within the right sidewall close to the south haulage underground opening were 79, 57, 49, and 29 mm, respectively, which accounted for 41%, 30%, 26%, and 15% of the total displacement of 191 mm between the 0 m and the 25 m-deep point, respectively (Figure 9b).

The displacements were mainly concentrated in the area from the surface (0 m) to 8–9 m deep in the surrounding rock mass. More precisely, the displacement within the 0–9 m-deep rock mass (101 mm = 153 mm − 52 mm) occupied 66% of the total (153 mm) of the left sidewall. Similarly, the displacement within the 0–8 m-deep rock mass (134 mm = 191 mm − 57 mm) accounted for 70% of the total (191 mm) at the right sidewall. Therefore, the deep holes post-grouting should be used to improve the strength and intactness of 8–9 m-deep surrounding rock mass.

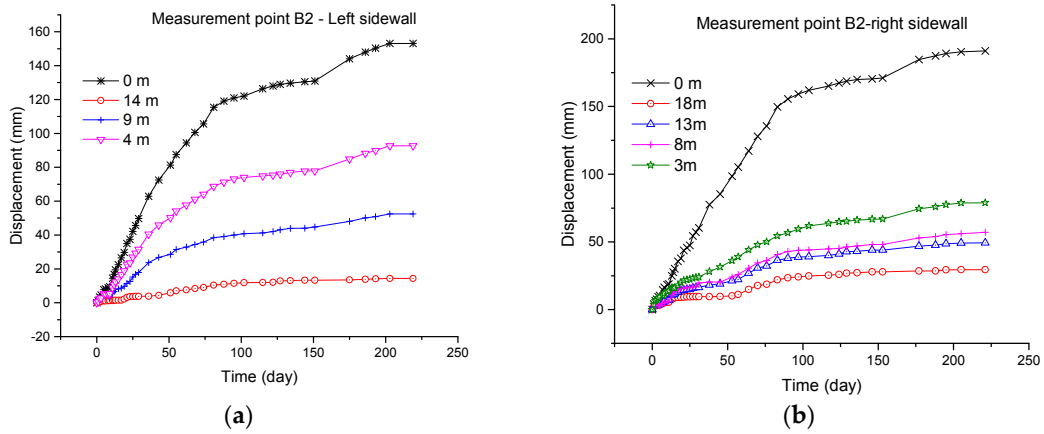

Figure 9. Displacements of deep surrounding rock at measurement point B2, 19 m away from fault FD108-1: (**a**) left sidewall; and (**b**) right sidewall.

However, the deep displacements of the inner surrounding rock were also evidently large, 49 mm at the 13 m-deep point and 29 mm at the 18 m-deep point. The loosened range of the inner surrounding

rock, i.e., the excavation damaged zone (EDZ) [24], due to stress redistribution after excavation, was over five times larger than the equivalent excavation radius (3 m) of the underground opening. The monitoring results indicated that the displacement of the inner surrounding rock was characterized by overall deformations on a large scale. The minimum pre-reinforcement range around the proposed opening should be 13–18 m.

In addition, the deep displacements within the right sidewall were much larger than those within the left sidewall. According to the construction and continuous monitoring, the deep displacement velocities suddenly accelerated twofold due to the delayed excavation of the south haulage underground opening. The monitoring indicates that subsequent excavation affects the stability of the south rail underground opening previously excavated, although the space between those two underground openings is approximately 30–40 m.

3.3. Factors Influencing Safe Excavation and the Stability of Deep Underground Openings

3.3.1. High In Situ Stress

The in-situ stress in the south underground opening was measured by hydraulic fracturing experiments performed in two long horizontal and vertical boreholes in the 800 m-deep connection roadway No. 5, where the rock mass was hard and intact. According to the results of the in-situ stress measurements, the magnitudes of the vertical stress and the maximum and minimum principal horizontal stresses were 28.78 MPa (σ_H), 16.34 MPa (σ_h), and 18.08 MPa (σ_v), respectively. The horizontal-to-vertical stress coefficient ($\lambda = \sigma_H/\sigma_v$ = 1.6) was more than 1.0. The in-situ stress field was dominated by horizontal tectonic stress. The south underground openings are in an extremely high-stress area. The orientation of the maximum horizontal stress is nearly in the EW direction. The directions of the maximum and minimum principal horizontal stresses are approximately perpendicular to and parallel to the south underground opening axis, respectively.

The higher the in-situ stress, the larger the deviator stress after excavation. The radial stress σ_{rr} decreases to 0 at the surface of the opening, whereas the tangential stress $\sigma_{\theta\theta}$ increases after excavation [25], resulting in a contradiction between the high stress and low rock mass strength and will inevitably lead to the rapid degradation of the surrounding rock mass after excavation. This is an important factor for deformations, failure, and instability of the deep underground opening through the large fault zones.

3.3.2. Large Fault Zones

The southern shear fault zones are large geological anomaly fault zones consisting of many large faults and small fractures, which are multi-period active fault zones that have undergone several tectonic movements including the Indosinian movement, Yanshan movement, and the neo-tectonic movement, that trend in the North–West–West (NWW) direction. The coal measure strata are frequently ruptured by faults, and the strata attitude varies strongly, leading to extremely complex geological conditions. The pilot underground excavation, passing through large fault FD108-1 to the south, showed that the surrounding rock mass was generally very loose and broken. The excavation-induced stress increase ahead of the tunneling face on the large fault would possibly cause the slip behavior of the large fault, affecting the excavation safety. In addition, the large deformations of the underground openings may also cause the delayed reactivation of faults, resulting in a wide range of rock mass instability. The fault reactivation will seriously threaten the tunneling safety and stability of the deep underground openings during excavation and operation.

Engineering practices showed that the roof collapse still occurred many times as the tunneling face approached the large fault FD108, even though 30 m-long pre-grouting boreholes and 15 m-long shed-pipe advanced pre-grouting supports were used. The pre-grouting reinforcement, such as ground surface pre-grouting (GSPG) should be used to improve the mechanical properties, including cohesion and internal frictional angle, of the large faults and regional engineering rock mass on a large scale.

3.3.3. Poor Physical-Mechanical Properties and Engineering Performance of the Surrounding Rock Mass

- Phase Composition Analysis by X-ray Diffraction (XRD)

Six argillaceous rock specimens were collected from the south haulage underground openings in the large fault zones in the Guqiao Coal Mine to analyze the mineral composition of the rock mass using the D/Max-3B XRD instrument (Rigaku Corporation, Tokyo, Japan).

Qualitative and quantitative analyses showed that the rock mass mainly consisted of clay minerals. The quantitative results are illustrated in Table 1 and Figure 10.

Table 1. Results of quantitative analysis of rock specimens' minerals (weight percentage).

No.	Description	Q	F	K	I	I/S	S	C	L	P	D	O
4	SJ52 + 75 m Roof	11.8	1.3	56.1	1.6	22.5	2.9			2.1		Other
5	SJ52 + 77 m Roof	13.7	0.8	55.9	2.9	18.6	4.3			1.4		Other
6	SJ52 + 77 m Floor	15.4	4.8	45.2	9.2	13.3	4.2	4.1	1.6	0.5	0.3	Other

Note: Q—Quartz: SiO_2; F—Feldspar: $(Na,Ca)AlSi_3O_8/(Na,K)AlSi_3O_8$; K—Kaolinite: $Al_4(OH)_8Si4O_{10}$, I—Illite: $KAl_2(OH)_2(AlSi)_4O_{10}$; S—Smectite: $(Na,Ca)_{0.7}(Al,Mg)_4(OH)_4(SiAl)_8\ O_{20}{\cdot}nH_2O$; I/S—Illite and smectite interstratified minerals; L—Siderite: $FeCO_3$; P—Pyrite: FeS_2; C—Calcite: $CaCO_3$; D—Dolomite: $(Ca, Mg)CO_3$, and O—Other.

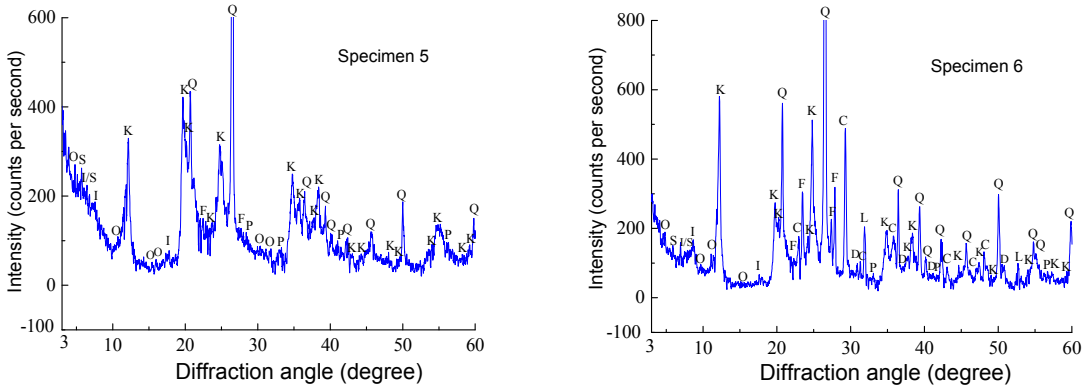

Figure 10. X-ray diffraction patterns of specimens: (**a**) Specimen 5; and (**b**) Specimen 6.

The Illite, Smectite, and Illite-Smectite interstratified minerals content in Specimens 4, 5, and 6 were 27%, 25.8%, and 26.7%, respectively. The kaolinite content in Specimens 4, 5, and 6 was 56.1%, 55.9%, and 45.2%, respectively. Therefore, the rock surrounding the south underground openings through the large fault zones consist of more than 70% clay minerals. The argillaceous rock contains substantial amounts of water-sensitive clay minerals and undergoes argillization when it is subjected to water.

- Argillization Experiment of Rock Mass Specimens with Water Immersion

Eight rock specimens (Table 2) were collected from the south haulage underground opening in large fault zones to conduct an argillization experiment with water immersion, as shown in Figure 11. Some parts of the saturated rock specimens were taken out and dried naturally to analyze weathering and disintegration of rock specimens. The weathering and disintegration of saturated argillaceous rock specimens are shown in Figure 12.

Table 2. Description of rock specimens with water immersion.

Specimen No.	Rock Specimen Description	Notes
1	Argillaceous rock from the left sidewall at SJ52 + 150 m	Indoor temperature was around 20 °C.
2	Argillaceous rock from the right sidewall at SJ52 + 150 m	
3	Argillaceous rock from the roof at SJ52 + 150 m	
4	Argillaceous sandstone from tunneling face at SJ52 + 150 m	
5	Argillaceous rock from the floor at SJ52 + 150 m	
6	Sandstone from the sidewall at SJ52 + 140 m	
7	Argillaceous rock from the roof at SJ52 + 140 m	
8	Argillaceous rock from the floor at SJ52 + 140 m	

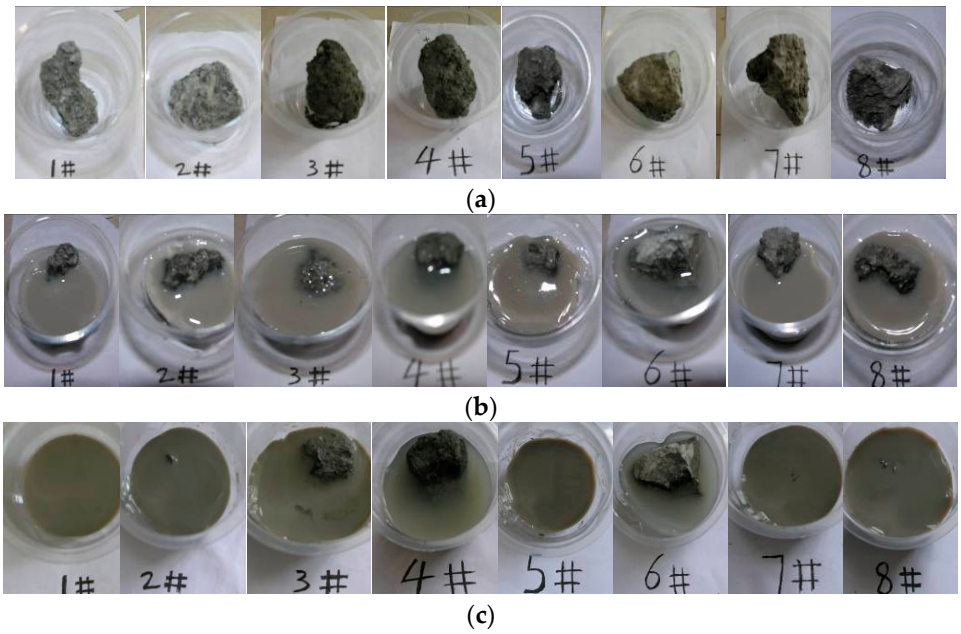

Figure 11. Argillization experiment process of rock specimens with water immersion: (**a**) condition of specimens before water immersion; (**b**) conditions of specimens with water immersion half a day later; and (**c**) condition of specimens with water immersion one day later.

Figure 12. Weathering and disintegration of saturated argillaceous rock.

As shown in Figures 11 and 12, argillaceous rock specimens were in full argillization after one day with water immersion, except Specimens 4 and 6, indicating that argillaceous rock containing substantial amounts of water-sensitive clay minerals will undergo evident softening, argillization, swelling, dissolution, and weakening when in contact with water and will easily disintegrate and weather after air drying. The experimental results show that the argillaceous rock, in the south underground openings through large fault zones, is hydrophilic swelling soft rock, sensitive to disintegrating and weathering, with a high erosion rate. Groundwater seepage and construction water should be a focus during excavation and support.

- Low Rock Mass Strength

The excavation was subjected to a series of faults from north to south in the deep underground openings. The small faults and fractures developed well with argillaceous gouge infilling. The rock mass was extremely broken in geological anomaly fault zones. The strength of the surrounding rock is extremely low. The roof collapses can be easily attributed to the broken soft rock mass without stand-up time after excavation. According to the classification of surrounding rock in rock roadways for coalmines, the classification of the surrounding rock of the south underground openings through the fault zones is category V [26–28]. The compressive strength of rock mass was generally less than 1.6 MPa.

- Poor Engineering Performance of Rock Mass

Borehole image monitoring was completed to detect the fracture conditions and analyze the quality of the grouting effect in the roof after post-grouting. The fractures, especially within 4–8 m-deep surrounding rock, remained extremely developed after 3 m-deep and 8 m-deep holes post-grouting with cement (Figures 13 and 14). The borehole image monitoring results indicated that the groutability of the cement-matrix grout materials was extremely poor in the argillaceous rock containing substantial amounts of clay minerals, due to their low permeability and self-sealing properties, as argillaceous rock swells when it meets water, thus closing fractures [29–31]. The common cement-matrix grout can only penetrate fractures of pores wider than 0.1 mm due to its large particle size [32]. Chemical materials should be further adopted for deep holes post-grouting reinforcement.

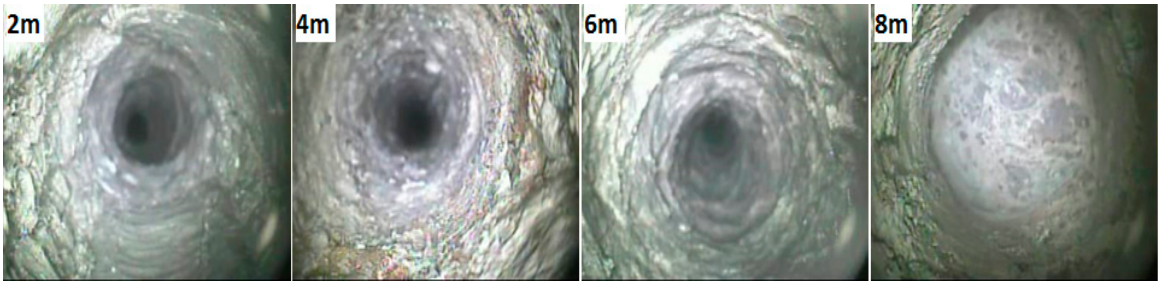

Figure 13. Borehole image monitoring in the roof after 3 m-deep holes post-grouting with Portland cement.

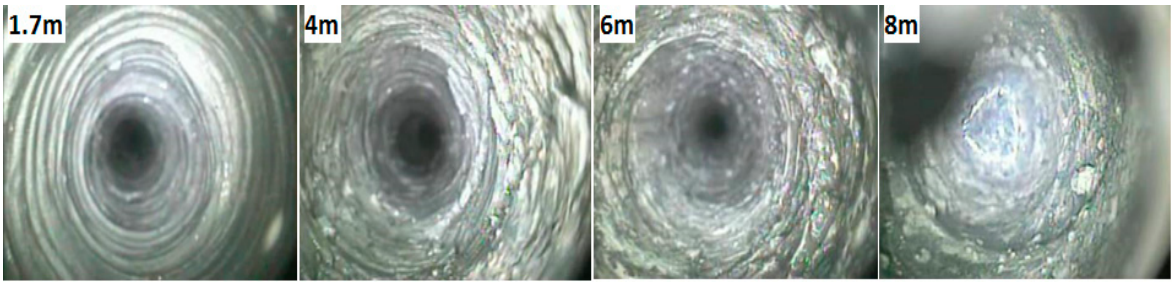

Figure 14. Borehole image monitoring in the roof after 8 m-deep holes post-grouting with superfine cement.

Figure 15 presents the curve of the axial loads of cables at SJ52 + 92 m during re-excavation when cable installation occurred before shotcrete and 3 m-deep holes post-grouting. The axial loads of cables first increased but then suddenly decreased. The axial loads of the cables underwent plummeting and unloading phenomena. The anchor-ability of cables within argillaceous surrounding rock was extremely poor.

Because of the gap and the broken rock mass behind the anchor cable plates, the high pre-tension force was difficult to preload to the cables that were installed before shotcrete and post-grouting. Cables were not able to effectively reinforce the rock mass in time because of the low pre-tension and

broken rock mass. Because the argillaceous surrounding rock mass mainly consists of water-sensitive clay minerals and excessive frequent groundwater inflow, the cables were often installed and anchored in the soft broken surrounding rock. The low pre-tension of the cables and the failure of rock mass around cable boreholes led to the plummet and unloading phenomena of the axial loads of cables. The strength and bearing capacity of argillaceous rock mass around underground openings with bolt and cable support would be significantly additionally lower during its argillization process due to groundwater seepage [33]. This would result in the failure of the bolting-reinforced structure and seriously threaten the long-term stability of the underground openings.

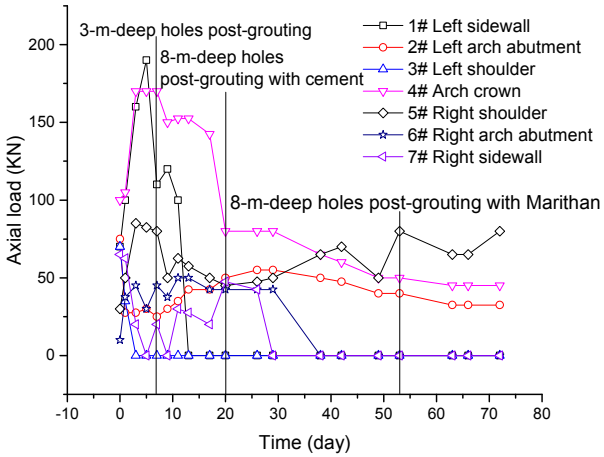

Figure 15. Axial loads of cables installed before shotcrete and 3 m-deep holes post-grouting during re-excavation.

3.3.4. Groundwater Inrush and Coal and Gas Outburst

The aquifer in the water-bearing Cenozoic loose strata on the bedrock that was dislocated by faults is rich aqueous. If the main faults, acting as groundwater inrush channels, are reactivated under the dynamic pressure resulting from the excavation, the groundwater inrush from the Cenozoic aquifer will threaten tunneling safety during excavation.

During the pilot excavation, excessive groundwater inflow, frequently associated with faults and fractures, often occurred. The groundwater inrush inflow of 10 m^3/h or more occurred more than 15 times. The maximum water inflow was up to 60 m^3/h with a temperature of approximately 42 °C. The normal water inflow of the complete excavation reached 5 m^3/h. The excessive groundwater inflow and seepage not only threatens tunneling safety during excavation but also continues to deteriorate the strength and deformation characteristics of the rock mass over time, and decreases the stability of deep underground openings in argillaceous rock [34]. The influence of groundwater on the argillaceous rock contains two main aspects: the mechanical action of water on the surrounding rock, including the hydrostatic pressure of the effective force and the dynamic water scouring effect, and the physical and chemical action of water on the rock mass, including softening, argillization, dissolution, and swelling [35,36].

In addition, the phenomenon of gas emission exists in advanced geological boreholes ahead of the tunneling face, and the maximum gas concentration was up to 10%. Owing to the influence of the faults, the excavation will pass through multiple coal seams, including coal seam 13-1 with coal and gas outburst risk and coal seam 11-2 with high rich gas [37], which also seriously threaten the accomplishment of a safe excavation.

4. Control Countermeasures for Deep Underground Openings through Large Fault Zones in Argillaceous Rock

Because of the geo-hazards encountered and potential fault slip behavior during deep underground excavation in large fault zones, providing adequate support or reinforcement to the rock

mass with sufficient speed after excavation is almost impossible. Reinforcing the rock mass in advance of excavation should be practical and adopted. In addition, extra reinforcement should be provided as part of the normal cycle, in anticipation of higher stresses being imposed on the rock at a later stage during the service life of the opening.

Many underground support schemes, such as the single-pilot heading method and long boreholes pre-grouting, were used during the industrial test of the pilot excavation of the deep underground openings through the large geological anomaly fault zones. However, various geological disasters still occurred during previous excavations, such as roof collapse, water inrush and debris flow. Engineering practices have shown that the geological conditions of underground openings are extremely complex.

According to the deformations and failure characteristics of the surrounding rock, the factors influencing safe excavation, underground opening stability, and geo-hazards encountered during the pilot excavation, a coordinated control technique method, including improvement of regional lithology, such as GSPG, primary enhanced control measures of the surrounding rock, and secondary enclosed support, should be adopted to ensure tunneling safety and the long-term stability of deep underground openings through large fault zones in argillaceous rock.

4.1. Regional Strata Reinforcement Technique—GSPG

GSPG involves injection of cement, or clay-cement, chemical liquid grouting materials into faults, fractures or dissolution cavities within water-bearing strata using mechanical methods [38]. The purposes of grouting are to block water-bearing conduits, control groundwater inflow, improve the regional engineering rock mass stability, and ensure safety during excavation and operation of deep underground openings. GSPG should be used to reinforce the regional engineering rock mass between the northern roof collapse location close to fault FD108 and the southern collapse. Boreholes are usually inside and/or outside the proposed excavated diameter of the south haulage underground opening. The detailed parameters and the reinforcement effect of GSPG and its influence on the stability of deep underground openings have been previously studied [21]. After the quality assessment of the GSPG effect, it is determined whether the proposed excavated zone pre-reinforcement technique, with underground long boreholes and shed-pipe advanced grouting support, should still be used. Short cycle chemical grouting pre-reinforcement should still be performed to prevent the roof and the tunneling face from collapsing during excavation. In addition, gas and water drainage exploration must be implemented to eliminate gas outbursts, groundwater inrush, and ensure tunneling safety.

4.2. Primary Enhanced Control Measures of the Surrounding Rock after Excavation

Rock mass is very broken in geological anomaly fault zones. The strength of the surrounding rock is extremely low. The roof collapses easily due to the broken soft rock mass not having stand-up time after excavation. Owing to the extremely dramatic initial deformations and complex geological conditions, enclosed support measures cannot be constructed immediately at the tunneling face after excavation.

Based on regional strata reinforcement, pre-grouting reinforcement, etc., completing primary enhanced control measures of the surrounding rock (heavy U36-shaped steel sets (36 kg/m steel), shallow holes post-grouting with superfine cement, bolts and long cables, and deep holes post-grouting with chemical material) should be aligned with the short cycle construction steps to control the dramatic initial deformations after excavation.

The U36-shaped steel sets are used first to ensure roof safety after excavation. Shotcrete lining and shallow holes post-grouting with cement should then be applied to seal the rock surface, inhibit weathering processes, fill the pore space behind the steel sets, and reinforce the shallow rock mass. Afterward, the high strength and pre-stressed thread steel bolt support system, combined with the long pre-stressed anchor cables, are installed. After that, deep holes post-grouting with chemical material, such as a novel polyurethane grouting material like the Marithan® polyurethane strata injection system [39,40], should be used to block fracture water from seeping, improve the intactness of

rock mass, and prevent the deep argillaceous surrounding rock mass from argillization. Marithan® is a flexible polyurethane product consisting of resin grout and catalyst, particularly well-suited for the reinforcement of fractured rock mass, the stabilization of water-bearing strata, and water stoppage. The product has high adhesive strength, outstanding mechanical properties, and good flexibility, creating an excellent bond with rock mass, which is maintained through the service life of the workplace. According to laboratory experimentation, the average uniaxial compressive strength, tensile strength, shear strength, and cohesion are 65.8 MPa, 41.5 MPa, 29.7 MPa, and 10.2 MPa, respectively [28].

The particle size distribution of Marithan® grout was observed by using a Mastersizer 2000 mercury porosimeter, as shown in Figure 16. The average particle sizes of Marithan® resin and catalyst are 2.95 nm and 825.6 nm, respectively. The maximum frequency size of Marithan® resin and catalyst (d^{max}) are 2.69 nm and 615.14 nm, respectively, while the particle sizes of the grout cumulative distribution curve corresponding to 95% (d_{95}) for resin and catalyst are 3.62 nm and 824.99 nm, respectively. According to the groutability principle of fracture or porous mediums, the width of the fractures or pores the grout could be injected into is bigger than triple the grouting material particle size [41]. The particle sizes over triple the d^{max} and d_{95} on the cumulative distribution curve of Marithan® resin are 8 nm ($R^{3\times d_{max}}$) and 11 nm ($R^{3\times d_{95}}$), respectively. Therefore, the Marithan® grout can be injected into fine fractures or pores of 11 nm in width, the groutability of which is obviously higher than cement-matrix grout ($\geq$0.1 mm). When Marithan® is injected into the strata, the low-viscosity mixture remains in a liquid state for several seconds, penetrates small fine fractures and expands, thus effectively reinforcing and sealing the area [42].

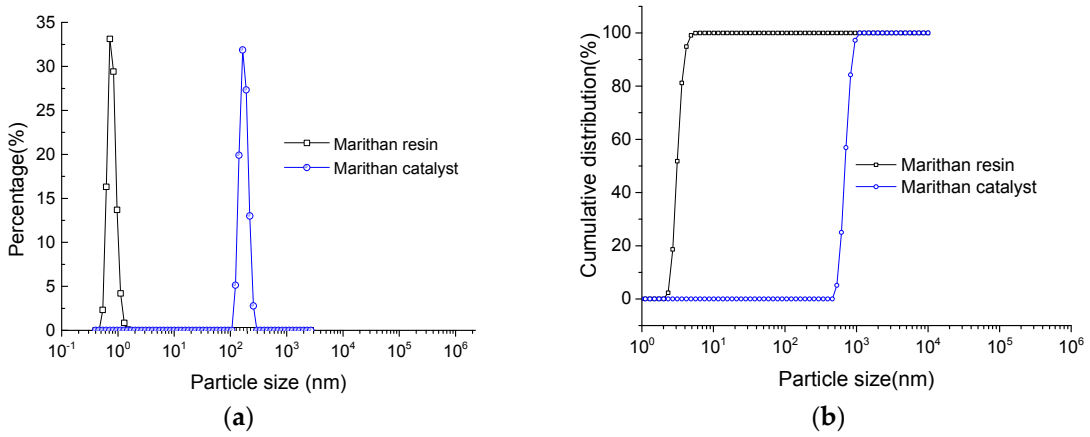

Figure 16. (**a**) Particle size distribution; and (**b**) cumulative particle size distribution of Marithan® grout.

4.3. Floor Grouting Reinforcement Technique with Pressurization and Progressive Depths

The floor heave of the underground openings is critical. Field measurements during the pilot excavation indicated that the displacement and velocity of the floor were up to 2901 mm and 80 mm/day, respectively. The floor must be reinforced given the destructive floor heave. However, the holes drilled in the floor are always subjected to collapse because of the soft broken argillaceous rock mass and its argillization. The bolts and cables cannot be installed in the floor.

Based on the industrial testing of the floor reinforcement in the south haulage underground opening, we proposed the floor grouting reinforcement technique with pressurization and progressive depths in argillaceous rock. Grouting depths in the floor successively increased from shallow to deep, and the corresponding grouting pressure also progressively increased (Figure 17). The array pitch and the water-to-cement ratio for 2.5 m-deep, 4.5 m-deep, and 6.5 m-deep holes grouting were all 1600 mm and 1:1, respectively. The array pitch of 8 m-deep holes with grouting with chemical material (Marithan®) was 2000 mm. The earlier shallow holes grouting not only reinforces the shallow rock mass but also forms a stop-grouting layer for subsequent deeper drilling holes grouting and solves the

problem of wall collapse in deeper holes. The 8 m-deep holes with grouting with chemical material (Marithan®) reinforces the deep rock mass in the floor and forms a large joint bearing ring with the reinforced deep rock mass in the roof and sidewalls. This technique effectively strengthens the floor in the large faults in argillaceous rock. The displacement velocity of the floor decreased to 0.7 mm/day on average, providing a foundation for secondary enclosed support measures for the long-term stability of the surrounding rock.

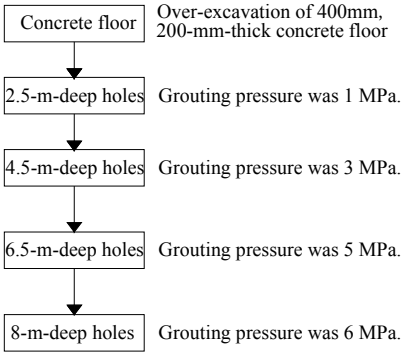

Figure 17. Industrial test process diagram of floor grouting reinforcement.

4.4. Secondary Enclosed Support

Given the significant creep behavior of the deformations and the long-term stability of the deep underground openings in the large faults in argillaceous rock, the secondary enclosed support measures, such as enclosed heavy U36-shaped steel sets and precast reinforced steel plate concrete segments, should be used. The buffer space between the secondary enclosed support structure and the primary enhanced control measures should be filled with backfilling materials to enable the pressure to evenly act on the backfilling layer and the support structure.

5. Re-Excavation of Deep Underground Openings through Large Fault Zones and Field Measurements

5.1. Support Schemes

The deformations and failure of the deep underground openings before re-excavation were extremely serious (Figure 18).

Figure 18. Failure of the deep underground openings through large fault zones in argillaceous rock.

The areas of the residual cross-sections were less than 4 m^2. Most cross-sections of the deep underground openings in the large fault zones were closed. The underground opening was re-excavated by hand air drill. The optimized support measures during re-excavation are illustrated as follows.

5.1.1. Short Cycle Chemical Grouting Pre-Reinforcement

Short cycle pre-grouting with chemical material (Marithan®) was performed to further reinforce fractured rock mass and prevent the tunneling face from collapsing (Figure 19). The lengths of grouting boreholes and pipes were 8000 mm and 6000 mm, respectively. The diameter of the grouting boreholes was 42 mm. The grouting pressure was 1–3 MPa.

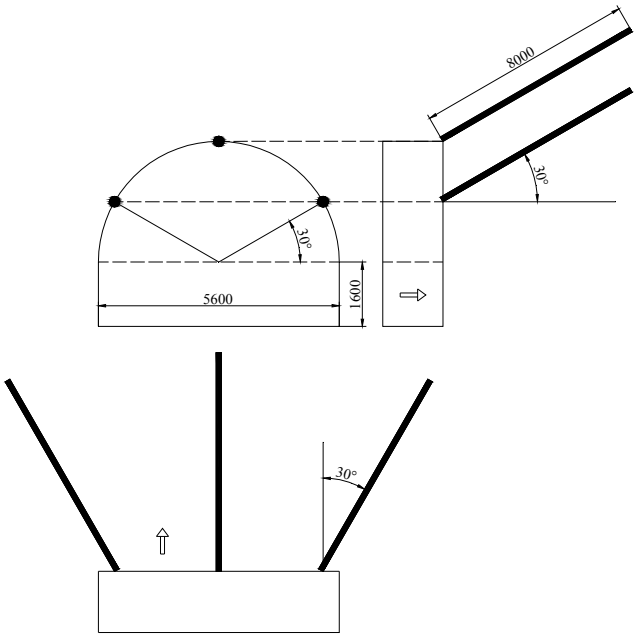

Figure 19. Layout diagram of short cycle chemical grouting pre-reinforcement.

5.1.2. U36-Shaped Steel Sets

U36-shaped steel sets with intervals of 400 mm were installed after excavation. The net cross-section of the steel sets was 5600 mm in width and 4400 mm in height. Two high-strength thread steel leg-locker bolts were installed in time to fix the leg of the steel set in the corner. The diameter and length of the bolts were 22 mm and 2800 mm, respectively. The torque of each bolt was not less than 200 Nm.

5.1.3. Cable Beams in Sidewalls

Pre-stressed anchor cable beams (Figure 20) composed of cables and strips of I-steel No. 11 were installed in the sidewalls after four U-shaped steel sets were finished. The diameter and length of the cables were 21.8 mm and 8200 mm, respectively. The pre-tension force of 100 kN was preloaded to cables to achieve high pre-stress to reinforce the sidewalls and restrict the deformations of the U-shaped steel sets.

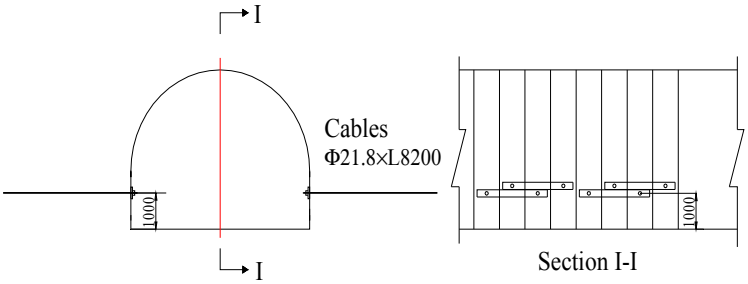

Figure 20. Layout diagram of I steel cable beams during re-excavation.

5.1.4. Primary Shotcrete

Primary shotcrete was performed up to the tunneling face to seal the rock surface and fill the pore space behind the steel sets after every five U-shaped steel sets were finished. The thickness was 50–70 mm. The shotcrete was composed of ordinary Portland cement, sand, and gravel mixed with water. The weight ratio of cement, sand, and gravel was 1:2:2, and the water-to-cement ratio was 45%. The strength grade of the ordinary Portland cement was 42.5 MPa.

5.1.5. Shallow Holes Post-Grouting with Superfine Cement

Shallow holes post-grouting with superfine cement was completed after shotcrete (Figure 21). The lengths of the grouting pipes and boreholes were 2000 mm and 3000 mm, respectively, and the array pitch was 3200 mm. Grouting pressure was generally not more than 3 MPa. The strength of the superfine cement was 62.5 MPa. The water-to-cement ratio was 0.8–1.0. The distance of shallow holes post-grouting relative to the tunneling face was less than 6 m.

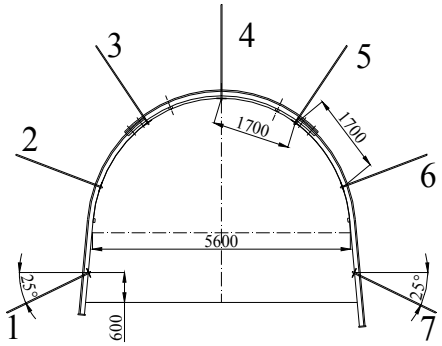

Figure 21. Pipe layout diagram of 3 m-deep holes post-grouting during re-excavation.

5.1.6. High-Strength and Pre-Stressed Bolts

Seventeen high-strength pre-stressed bolts (left-hand twist and IV class thread steel HRB500) were used to reinforce each cross-section (Figure 22). The diameter and length of the bolts were 22 mm and 2800 mm, respectively. The interval and array pitch of the bolts were 800 mm and 800 mm, respectively. The torque of each bolt was not less than 200 Nm.

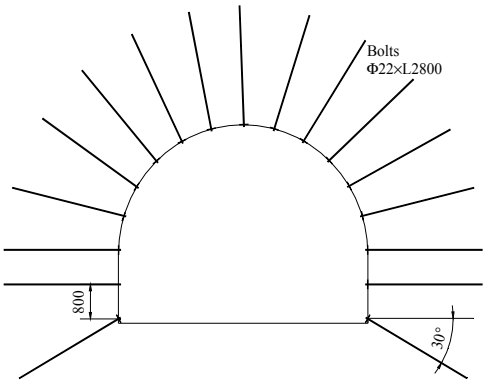

Figure 22. Layout of bolts.

5.1.7. Pre-Stressed Cables

Seven pre-stressed cable beams (Figure 23), consisting of cables and T steel strips, were applied installed perpendicular to the roadway axis direction. The diameter of the cables was 21.8 mm. The length of the cables with an exposed length of approximately 200 mm was 8200 mm. A high

pre-tension force of approximately 100 kN should be preloaded to cables to achieve the high pre-stress during post-excavation installation. The delaying distance of cable installation relative to the tunneling face was less than 8 m.

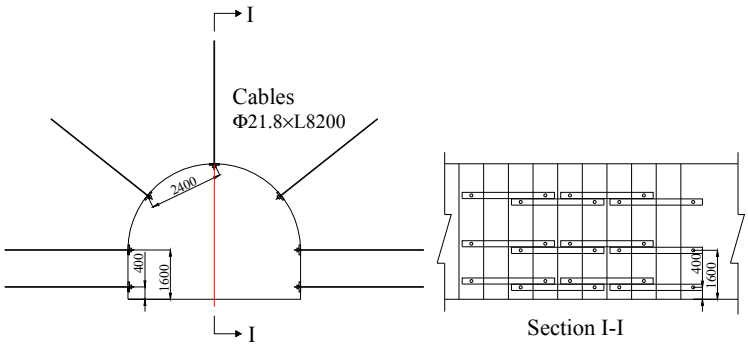

Figure 23. Layout diagram of the cable beams.

5.1.8. Secondary Shotcrete

Secondary shotcrete was used to seal the deformation-induced fractures and pore space of the boreholes after cable installation. The thickness was 50–70 mm. The shotcrete materials were the same as those of primary shotcrete. The distance of the secondary shotcrete relative to the tunneling face was less than 10 m.

5.1.9. Deep Holes Post-Grouting with Chemical Material

Deep holes post-grouting with Marithan® were bored after secondary shotcrete (Figure 24). The lengths of grouting pipes and boreholes were 6000 mm and 8000 mm, respectively. The array pitch was 3200 mm. The grouting pressure was 6–8 MPa.

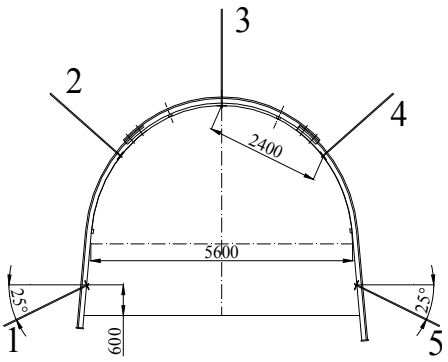

Figure 24. Pipe layout diagram of 8 m-deep holes post-grouting during re-excavation.

To improve the grouting effect, deep post-grouting was conducted by a repeated grouting method with alternating intervals; i.e., the odd array holes grouting was first completed along the opening axis direction. Afterward, the grouting of the remaining even array holes was conducted. In addition, the deep holes post-grouting sequences at the same cross-section were from holes No. 1 and No. 5 in the corners, then holes No. 2 and No. 4 in the shoulders, to the last hole No. 3 in the arch crown.

5.1.10. Secondary Enclosed Support

The floor grouting reinforcement technique with pressurization and progressive depth parameters were the same as those in Section 4. The secondary enclosed support should be further designed and implemented after floor grouting reinforcement to ensure the long-term stability of the underground openings through large fault zones in argillaceous rock, given the creep and time-dependent behavior.

5.2. Field Measurements

To analyze the reliability of the support parameters for the deep underground opening during re-excavation, field measurements such as surface displacements, bedding separation of roof strata, axial load monitoring of cables, and borehole image monitoring were recorded, discussed and compared with the monitoring results during the pilot excavation.

5.3. Results and Discussion

- Surface Displacements

The field measurements confirmed that cable reinforcement after shotcrete and 3 m-deep holes post-grouting could reduce the displacements of the surrounding rock. For example, the maximum sidewall-to-sidewall and roof-to-floor displacement velocities were 25 mm/day and 46 mm/day, respectively, on the first day after re-excavation. The corresponding displacement velocities visibly decreased to 13 mm/day on the seventh day and 15 mm/day on the ninth day, respectively, after the cables around the measurement point at SJ52 + 24 m were installed on the sixth day after re-excavation (Figure 25).

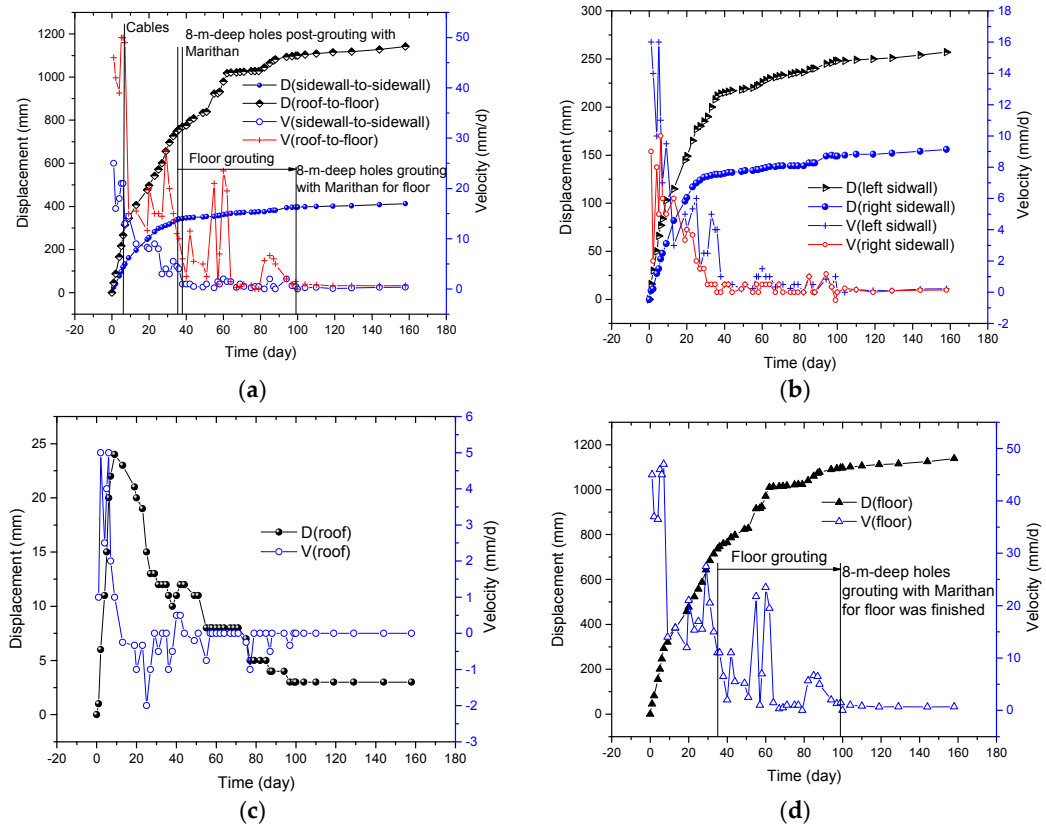

Figure 25. Curves of displacements and velocities versus time during re-excavation: (**a**) sidewall-to-sidewall and roof-to-floor; (**b**) left and right sidewalls; (**c**) roof; and (**d**) floor.

The 8 m-deep holes post-grouting, reinforced with chemical material (Marithan®) for the sidewalls and the roof around the monitoring point, were installed on the 35th day and finished on the 38th day after re-excavation, further reducing the displacement velocities. For instance, the sidewall-to-sidewall and roof-to-floor displacement velocities were 4.5 mm/day and 11 mm/day on the 35th day, respectively, which then decreased to 1 mm/day and 6 mm/day on the 38th day, respectively. Thirty-eight days later, the sidewall-to-sidewall and roof-to-floor displacements were 344 mm and 770 mm, respectively. Afterward, the deformations of the surrounding rock were rheological (creep and time-dependent), but the displacement creep rate of the left sidewall, right sidewall, and roof were

less than 1 mm/day. Deep holes post-grouting reinforced with chemical material played an important role in the stability of the deep underground opening.

The floor grouting reinforcement technique with pressurization and progressive depths was started on the 35th day and finished on the 99th day. The floor displacement velocity experienced dramatic fluctuations between 0 and 23.5 mm/day during the floor grouting due to the construction disturbance of the drilling boreholes. Ninety-nine days later, the floor displacement velocity decreased to below 1 mm/day with an average of 0.7 mm/day. The floor grouting reinforcement technique provides a foundation for secondary enclosed support measures for the long-term stability of the surrounding rock.

A total of 158 days later, according to Figure 25, the creep rates of sidewall-to-sidewall, roof-to-floor, the left sidewall, the right sidewall, the roof, and the floor were 0.36 mm/day, 0.71 mm/day, 0.21 mm/day, 0.14 mm/day, 0 mm/day, and 0.71 mm/day, respectively. The total corresponding displacements were 413 mm, 1142 mm, 257 mm, 156 mm, 3 mm, and 1139 mm, respectively. In addition, the displacements showed asymmetry during re-excavation. The displacements of the left sidewall (257 mm) and the floor (1139 mm) were much larger than those of the roof and the right sidewall, which represented 62% and 99% of the roof-to-floor (1142 mm) and sidewall-to-sidewall (413 mm) deformations, respectively. Compared to the displacements during the pilot excavation, the displacements decreased considerably during re-excavation. Compared with the displacements of sidewall-to-sidewall (1852 mm) and roof-to-floor (3259 mm) at measurement point C7 during the pilot excavation, the displacements decreased considerably by 78% and 65%, respectively, during re-excavation. The support effect is shown in Figure 26.

Figure 26. Support effect after 8 m-deep holes post-grouting with Marithan®.

- Borehole Image Monitoring

Compared to the grouting effect of 3 m-deep holes post-grouting with cement and 8 m-deep holes post-grouting with superfine cement in the roof (Figures 13 and 14), borehole image monitoring showed that fractures were significantly reduced after 8 m-deep post-grouting with Marithan® (Figure 27), indicating that the chemical material is much better and more suitable for reinforcing argillaceous surrounding rock mass than cement grouting. Deep holes post-grouting with chemical material Marithan® could improve the intactness of argillaceous rock mass.

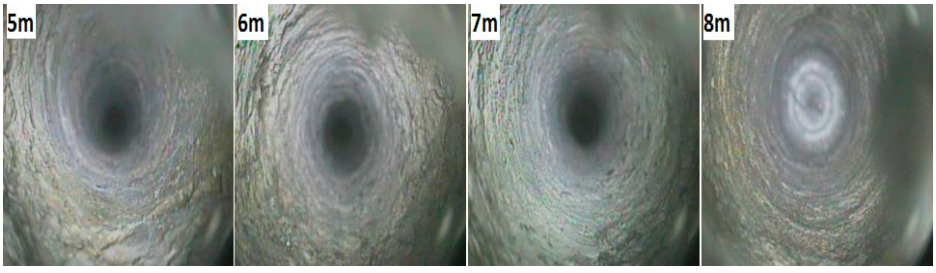

Figure 27. Borehole image monitoring in the roof after 8 m-deep holes post-grouting with Marithan®.

- Axial Load Monitoring of Cables

The 8 m-deep holes post-grouting with chemical material (Marithan®) around the monitoring cross-section of cables at SJ52 + 54 m were installed the 23rd and the 25th day, and were finished on the 46th day, after re-excavation. Compared to the anchor-ability of installed before shotcrete and the 3 m-deep holes post-grouting (Figure 15), the anchor-ability of cables within argillaceous surrounding rock was greatly improved when the cables were installed after shotcrete and 3 m-deep holes post-grouting (Figure 28). The 8 m-deep holes post-grouting with Marithan® reinforced the rock mass and further improved the anchor-ability of the cables.

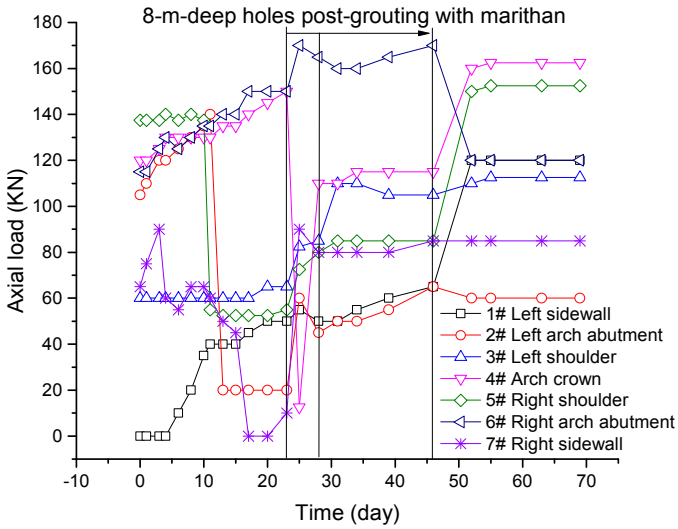

Figure 28. Axial loads of cables installed after shotcrete and 3 m-deep holes post-grouting during re-excavation using 8 m-deep holes post-grouting with Marithan®.

6. Conclusions and Research Prospects

The stability of deep underground openings during operation determines the sustainable safety production in underground coal mines. This work was a case study on the stability control of 800 m-deep underground openings in large fault zones in argillaceous rock that play a pivotal role in the sustainable development of the Guqiao Coal Mine in East China. The results were based on the analysis of long-term field measurements and engineering practices that provide valuable practical guidance for the stability control of deep underground openings in other coal mines with similar geological conditions, such as the Gubei and Panyidong Coal Mines in East China. Some conclusions and research prospects are summarized below.

6.1. Deformation and Failure Characteristics

Engineering practices and field measurements indicated that deformations and failure of the surrounding rock of deep underground openings in large fault zones are characterized by dramatic initial deformation, high long-term creep rate, obviously asymmetric deformations and failure, rebound of roof displacements, overall loosened deformations of deep surrounding rock mass on a large scale, and high sensitivity to engineering disturbance and water immersion.

6.2. Minimum Range of Pre-Grouting and Post-Grouting Reinforcement for Deep Underground Openings through Large Fault Zones

According to field measurements, the minimum pre-reinforcement range around the proposed deep underground opening through the large fault zones should be 13–18 m. Moreover, the minimum reinforcement range of deep holes post-grouting should be completed to improve the strength and intactness of the 8–9 m-deep surrounding rock mass.

6.3. Influencing Factors

The main factors influencing safe excavation and the stability of deep underground openings include large fault zones, high in situ stress, poor mechanical properties and engineering performance of the argillaceous surrounding rock mass, groundwater inrush, and gas outburst. The risks, including large fault reactivation, coal and gas outbursts, and groundwater inrush, seriously threaten tunneling safety during excavation. Ground surface pre-grouting (GSPG) should be completed to reinforce the regional engineering rock mass around the large fault FD108, between the northern and southern collapses, and eliminate fault reactivation and groundwater inrush hazards, as well as underground long advanced boreholes pre-grouting. The detection and drainage of groundwater and gas in advance, as well as strengthening management of groundwater and construction water should be conducted.

6.4. Pre-Grouting and Deep Holes Post-Grouting with a Novel Polyurethane Grouting Material

The experimental results show that the argillaceous rock consisting of over 70% clay minerals will undergo softening, argillization, disintegrating, and swelling when in contact with water seepage. Engineering practices indicate that the anchor-ability of cables before shotcrete and post-grouting, and groutability with cement-matrix materials in the argillaceous rock mass is extremely poor. Shotcrete should be applied to seal and support the rock surface to inhibit weathering processes after excavation. Pre-grouting and deep holes post-grouting with a novel polyurethane grouting material (Marithan®) should be used to block fracture water from seeping, and prevent the deep argillaceous rock mass from argillization. Field measurements during re-excavation indicated that deep holes post-grouting with Marithan® were not only able to improve the intactness of deep rock mass and prevent the argillaceous rock from argillization, but also improves the anchor-ability of cables in the fractured argillaceous rock mass.

6.5. Suggestions of Coordinated Control Techniques

According to the deformations and failure characteristics of the surrounding rock, the factors influencing the safe excavation and the stability and geo-hazards encountered during the pilot excavation, coordinated control techniques, including regional strata reinforcement technique such as GSPG, primary enhanced control measures of the surrounding rock, floor grouting reinforcement technique with pressurization and progressive depths, and secondary enclosed support are proposed and should be adopted to ensure the tunneling safety and long-term stability of deep underground openings through large fault zones in argillaceous rock.

6.6. Research Prospects

The influence of creep and time-dependent behavior on the stability of 800 m-deep underground openings was obtained in this study by only using field measurements. However, the obvious creep and time-dependent behavior of deep underground openings in argillaceous rock that results from the solid–liquid–gas-temperature coupling effect of deep rock mass, as well as the interaction with the underground openings is a complex issue that should be further investigated in the future using other methods such as numerical simulation.

Acknowledgments: This work was financially supported by the National Key Research and Development Program of China (Grant No. 2017YFC0603001), the National Natural Science Foundation of China (Grant No. 51704277), and the Project funded by China Postdoctoral Science Foundation (Grant No. 2017M621874). The authors would like to express appreciation to Liang YUAN in the Anhui University of Science and Technology, Quansheng LIU in the Institute of Rock and Soil Mechanics (Wuhan), Chinese Academy of Sciences and the staff at the Guqiao Coal Mine for their assistance during the field measurements. We also thank MDPI English Editing Service for improving the English text of this manuscript.

Author Contributions: All of the authors contributed extensively to the work. Deyu Qian proposed key ideas and wrote the manuscript. Nong Zhang provided some ideas and practice guidance in the research process. Dongjiang Pan, Zhengzheng Xie, Hideki Shimada, Yang Wang, Chenghao Zhang and Nianchao Zhang modified the manuscript.

Conflicts of Interest: The authors declare no conflict of interest.

References

1. Fu, F.; Liu, H.; Polenske, K.R.; Li, Z. Measuring the energy consumption of china's domestic investment from 1992 to 2007. *Appl. Energy* **2013**, *102*, 1267–1274. [CrossRef]
2. He, M.C.; Xie, H.P.; Peng, S.P.; Jiang, Y.D. Study on rock mechanics in deep mining engineering. *Chin. J. Rock Mech. Eng.* **2005**, *24*, 2803–2813. (In Chinese)
3. Kong, S.L.; Cheng, Y.P.; Ren, T.; Liu, H.Y. A sequential approach to control gas for the extraction of multi-gassy coal seams from traditional gas well drainage to mining-induced stress relief. *Appl. Energy* **2014**, *131*, 67–78. [CrossRef]
4. Wang, K.; Wei, Y.M.; Zhang, X. Energy and emissions efficiency patterns of Chinese regions: A multi-directional efficiency analysis. *Appl. Energy* **2013**, *104*, 105–116. [CrossRef]
5. National Bureau of Statistics of China. Available online: http://www.stats.gov.cn (accessed on 15 October 2015).
6. Huang, J.; Tian, C.; Xing, L.; Bian, Z.; Miao, X. Green and Sustainable Mining: Underground Coal Mine Fully Mechanized Solid Dense Stowing-Mining Method. *Sustainability* **2017**, *9*, 1418. [CrossRef]
7. Yang, W.; Lin, B.Q.; Qu, Y.A.; Li, Z.W.; Zhai, C.; Jia, L.L.; Zhao, W.Q. Stress evolution with time and space during mining of a coal seam. *Int. J. Rock Mech. Min. Sci.* **2011**, *48*, 1145–1152. [CrossRef]
8. Wang, L.; Cheng, Y. Drainage and utilization of Chinese coal mine methane with a coal-methane Co-exploitation Model: Analysis and Projections. *Resour. Policy* **2012**, *37*, 315–321. [CrossRef]
9. State Administration of Work Safety of China. Available online: www.Chinasafety.gov.cn (accessed on 15 October 2015).
10. Liu, Q.S.; Zhang, W.; Lu, X.L.; Fu, J.J. Safety monitoring and stability analysis of large-scale roadway in fault fracture zone. *Chin. J. Rock Mech. Eng.* **2010**, *29*, 1954–1962. (In Chinese)
11. Liao, Q.L.; Hou, Z.S.; He, X.D.; Dong, W.L.; Xiao, Q.B. Monitoring and analysis on the deformation of tunnel surrounding rock affected by fault. *Hydrogeol. Eng. Geol.* **2005**, *32*, 102–107.
12. Hao, Y.H.; Azzam, R. The plastic zones and displacements around underground openings in rock masses containing a fault. *Tunn. Undergr. Space Technol.* **2005**, *20*, 49–61. [CrossRef]
13. Schubert, W.; Riedmüller, G. Influence of faults on tunnelling. *Felsbau* **1997**, *15*, 483–488.
14. Jeon, S.; Kim, J.; Seo, Y.; Hong, C. Effect of a fault and weak plane on the stability of a tunnel in rock—A scaled model test and numerical analysis. *Int. J. Rock Mech. Min. Sci.* **2004**, *41*, 658–663. [CrossRef]
15. Russo, M.; Germani, G.; Amberg, W. Design and construction of large tunnel through active faults: A recent application. In Proceedings of the International Conference of Tunnelling and Underground Space Use, Istanbul, Turkey, 16–18 October 2002.
16. Lei, J.; Bai, M.Z.; Xu, Z.Y.; Zhang, A.J.; Huo, Y.H.; Wang, P.C. In-situ test on construction effect with freezing method for fault-crossing fragmentation zone in metro tunnel. *Chin. J. Rock Mech. Eng.* **2008**, *27*, 1492–1498. (In Chinese)
17. Zhang, N.; Xu, X.L.; Chen, Z.F.; Wang, C. Geological guarantee and construction controlling technique of main roadway crossing fault zone with 435-m fall. *Chin. J. Rock Mech. Eng.* **2008**, *27*, 3292–3297. (In Chinese)
18. Gao, Y.; Liu, D.; Zhang, X.; He, M. Analysis and Optimization of Entry Stability in Underground Longwall Mining. *Sustainability* **2017**, *9*, 2079. [CrossRef]
19. Zhang, Z.; Shimada, H.; Sasaoka, T.; Hamanaka, A. Stability control of retained goaf-side gateroad under different roof conditions in deep underground y type longwall mining. *Sustainability* **2017**, *9*, 1671. [CrossRef]
20. Qian, D.; Zhang, N.; Shimada, H.; Wang, C.; Sasaoka, T.; Zhang, N. Stability of goaf-side entry driving in 800-m-deep island longwall coal face in underground coal mine. *Arab. J. Geosci.* **2016**, *9*, 1–28. [CrossRef]
21. Qian, D.; Zhang, N.; Zhang, M.; Shimada, H.; Cao, P.; Chen, Y.; Wen, K.; Yang, S.; Zhang, N. Application and evaluation of ground surface pre-grouting reinforcement for 800-m-deep underground opening through large fault zones. *Arab. J. Geosci.* **2017**, *10*, 1–20. [CrossRef]
22. Wang, C.; Wang, Y.; Lu, S. Deformation behaviour of roadways in soft rocks in underground coal mines and principles for stability control. *Int. J. Rock Mech. Min. Sci.* **2010**, *37*, 937–946. [CrossRef]
23. Fabre, G.; Pellet, F. Creep and time-dependent damage in argillaceous rocks. *Int. J. Rock Mech. Min. Sci.* **2006**, *43*, 950–960. [CrossRef]
24. Blümling, P.; Bernier, F.; Lebon, P.; Martin, C.D. The excavation damaged zone in clay formations time-dependent behaviour and influence on performance assessment. *Phys. Chem. Earth* **2007**, *32*, 588–599. [CrossRef]

25. Liu, Q.S.; Kang, Y.S.; Bai, Y.Q. Research on supporting method for deep rock roadway with broken and soft surrounding rock in Guqiao Coal Mine. *Rock Soil Mech.* **2011**, *32*, 3097–3104. (In Chinese)
26. Yuan, L.; Xue, J.H.; Liu, Q.S.; Liu, B. Surrounding rock stability control theory and support technique in deep rock roadway for coal mine. *J. China Coal Soc.* **2011**, *36*, 535–543. (In Chinese)
27. Liu, Q.S.; Gao, W.; Yuan, L. *Surrounding Rock Stability Control Theory and Support Technique in Deep Rock Roadway for Coal Mine and Application*; Science Press: Beijing, China, 2010; pp. 77–82, 257–258. ISBN 978-7-03-026333-9. (In Chinese)
28. Qian, D. Countermeasures for Stability Control of Deep Underground Openings through Fault Zones in Argillaceous Rock. Ph.D. Dissertation, Kyushu University, Fukuoka, Japan, 2015.
29. Mánica, M.; Gens, A.; Vaunat, J.; Ruiz, D.F. A time-dependent anisotropic model for argillaceous rocks. Application to an underground excavation in Callovo-Oxfordian claystone. *Comput. Geotech.* **2017**, *85*, 341–350. [CrossRef]
30. Wang, L.L.; Bornert, M.; Yang, D.S.; Héripré, E.; Chanchole, S.; Halphen, B.; Pouya, A.; Caldemaison, D. Microstructural insight into the nonlinear swelling of argillaceous rocks. *Eng. Geol.* **2015**, *193*, 435–444. [CrossRef]
31. Wang, L.L.; Yang, R.W.; Chanchole, S.; Zhang, G.Q. The time-dependent swelling of argillaceous rock under resaturated conditions. *Appl. Clay Sci.* **2017**, *146*, 186–194. [CrossRef]
32. Guan, X.M.; Zhong, Q.F. Research on the Performance of Micro-fine Cement-based Grouting Material and Its Engineering Application. *Saf. Coal Mines* **2013**, *44*, 142–145. (In Chinese)
33. Zhao, Y.; Li, G.; Xu, X.; Yu, X. Transient process control technology for argillaceous roadway with water seepage. *Disaster Adv.* **2013**, *6*, 44–54.
34. Li, G.; Jiang, Z.; Lv, C.; Chao, H.; Gui, C.; Li, M. Instability mechanism and control technology of soft rock roadway affected by mining and high confined water. *Int. J. Min. Sci. Technol.* **2015**, *25*, 573–580. [CrossRef]
35. Vergara, M.R.; Triantafyllidis, T. Influence of water content on the mechanical properties of an argillaceous swelling rock. *Rock Mech. Rock Eng.* **2016**, *49*, 1–14. [CrossRef]
36. Yang, R.S.; Li, Y.L.; Guo, D.M.; Yao, L.; Yang, T.M.; Li, T.T. Failure mechanism and control technology of water-immersed roadway in high-stress and soft rock in a deep mine. *Int. J. Min. Sci. Technol.* **2017**, *27*, 245–252. [CrossRef]
37. Guo, H.; Yuan, L.; Shen, B.T.; Qu, Q.D.; Xue, J.H. Mining-induced strata stress changes, fractures and gas flow dynamics in multi-seam longwall mining. *Int. J. Rock Mech. Min. Sci.* **2012**, *54*, 129–139. [CrossRef]
38. Yang, C.L.; Wang, Z.M. Surface pre-grouting and freezing for shaft sinking in aquifer formations. *Mine Water Environ.* **2005**, *24*, 209–212. [CrossRef]
39. Li, L.P.; Li, S.C.; Zhang, Q.S.; Cui, J.S.; Xu, Z.H.; Li, Z. Experimental study of a new polymer grouting material. *Chin. J. Rock Mech. Eng.* **2010**, *29*, 3150–3156. (In Chinese)
40. Wang, H.P.; Gao, Y.F.; Li, S.C. Uniaxial experimental study on mechanical properties of reinforced broken rocks pre-and-post grouting. *Chin. J. Undergr. Space Eng.* **2007**, *3*, 27–31. (In Chinese)
41. Pan, D.; Zhang, N.; Han, C.; Yang, S.; Zhang, C.; Xie, Z. Experimental study of imbibition characteristics of silica sol in coal-measure mudstone matrix. *Appl. Sci.* **2017**, *7*, 300. [CrossRef]
42. Zhang, D.L.; Fang, Q.; Lou, H.C. Grouting techniques for the unfavorable geological conditions of Xiang'an subsea tunnel in China. *J. Rock Mech. Geotech. Eng.* **2014**, *6*, 438–446. [CrossRef]